ELSEVIER

Journal of Structural Geology 26 (2004) 1989–2009

JOURNAL OF STRUCTURAL GEOLOGY

www.elsevier.com/locate/jsg

Recycling of foliations during folding

A.P. Ham, T.H. Bell*

School Earth Sciences, James Cook University, Townsville, Qld. 4811, Australia

Received 10 September 2003; received in revised form 10 April 2004; accepted 12 April 2004

Available online 2 July 2004

Abstract

Bedding on the limbs of early-formed regional folds generally lies oblique to the major directions of bulk shortening in the crust, that is, the horizontal and vertical. During subsequent deformations, matrix foliations on at least one limb of these folds may start to form but then be destroyed by reactivation of the bedding causing decrenulation and rotation into parallelism with the compositional layering. Consequently, the schistosity parallel to bedding ($S_0//S_1$) in multiply deformed rocks contains the relics of many deformation events, and the two or three oblique foliations record only the very youngest history. This lengthy early history is preserved as inclusion trails within porphyroblasts. Recycling of foliations depends on the shear sense acting on any newly developing foliation and the orientation of this foliation relative to $S_0//S_1$. For some orientations and combinations of shear senses, both limbs of a pre-existing fold can be reactivated from the commencement of a new deformation event. This can result in the decrenulation and obliteration of a new foliation that is beginning to form before it shows any significant degree of development. For other combinations, one limb of a pre-existing fold will behave in this manner whereas a new foliation does develop fully on the other limb. However, subsequent phases of deformation switch which limb shears vs. develops an oblique new cleavage rotating the earlier formed oblique foliation into parallelism with $S_0//S_1$.

Keywords: Foliation reactivation; Fold mechanisms; Crenulation cleavage; Shear sense

1. Introduction

Unravelling the history of complexly deformed and metamorphosed terrains requires determination of the relationship between large-scale folds and multiple foliations that have developed through successive deformations. Typically this is achieved by establishing overprinting between successive foliations, and the analysis of the geometric relationships between these foliations and the macro scale folds. However, in highly deformed terrains, where the dominant foliation is sub parallel to compositional layering ($S_0//S_1$), correlating foliations is commonly problematic. Reactivation of the bedding or compositional layering tends to destroy newly developing foliations and rotate earlier formed ones that are still oblique to $S_0//S_1$ into parallelism with it (Bell, 1986). Preservation of relics of earlier foliations in rocks where the younger deformation has not been strongly partitioned, or in the strain shadows of large competent bodies, such as granites, or small scale ones, such as porphyroblasts, makes successful correlation of foliations difficult from outcrop to outcrop. Geometric analysis from field mapping of such areas typically is insufficient, as further detailed microstructural analysis of the inclusion trails within porphyroblasts, where they are available, generally reveals more complex histories than inferred from matrix relationships alone (Bell et al., 2003).

Inclusion trail geometries within porphyroblasts can be used to establish the relative timing of foliations relative to one another and larger scale folds. A decade of quantitative work has shown that inclusion trails have sigmoidal, staircase and spiral geometries that form around one or more foliation inflexion/intersection axes in porphyroblasts (FIAs) in a single sample (e.g. Bell et al., 1998), but their asymmetry does not necessarily switch in any classic manner across fold hinges (Bell et al., 2003). Indeed, it has become apparent that geometrically simple macroscopic folds commonly show a very complex microscopic history of development (Adshead-Bell and Bell, 1999; Hickey and Bell, 2001; Bell et al., 2003). Inherent to foliation–fold relationships is the manner in which strain accumulates during deformation and, in particular, what

* Corresponding author. Tel.: +61-7-4781-4766; fax: +61-7-4725-1501.
E-mail address: tim.bell@jcu.edu.au (T.H. Bell).

0191-8141/$ - see front matter © 2004 Elsevier Ltd. All rights reserved.
doi:10.1016/j.jsg.2004.04.003

fold mechanism(s) has operated. There are two contrasting kinematic models for how this occurs:

1. During flexural folding, non-coaxial deformation is accommodated by shear on folded layers, with little or no shear on differentiated axial plane crenulation cleavages. Bulk shortening and fine scale buckling (Fig. 1a–d) causes crenulation of the earlier cleavage (S_n) followed by the development of a fold (Fig. 1e; Gray, 1979; Twiss and Moores, 1992). The clockwise (CW) buckling rotation of the right limb in Fig. 1c and e is accommodated by anticlockwise (ACW) flexural slip on the foliation being folded (Fig. 1d and f). These processes compete in their effect on the orientation of S_{n+1} as they rotate it opposite directions, generally to little effect, and a long and short limb develop (Fig. 1d and f). Dissolution and solution transfer, generally of the long limb of these fine scale crenulations occurs (the limb closest in orientation to the axial plane), developing a differentiated crenulation cleavage S_{n+1}, with the shear shown in Fig. 1f and h being apparent rather than real. Any actual synthetic shear (CW in Fig. 1f and h) along S_{n+1} develops late during folding.
2. During folding due to progressive bulk inhomogeneous shortening the deformation partitions into zones of progressive shortening and shearing (Fig. 2a and b; Bell, 1981). The zones of progressive shearing become crenulation cleavage seams (S_{n+1}) and the zones of progressive shortening become crenulation hinges as shown in Fig. 2b (Bell and Hickey, 1997; Bell et al., 2003). Non-coaxial synthetic progressive shearing (ACW in Fig. 2b) is partitioned in an anastomosing manner around zones of near coaxial progressive

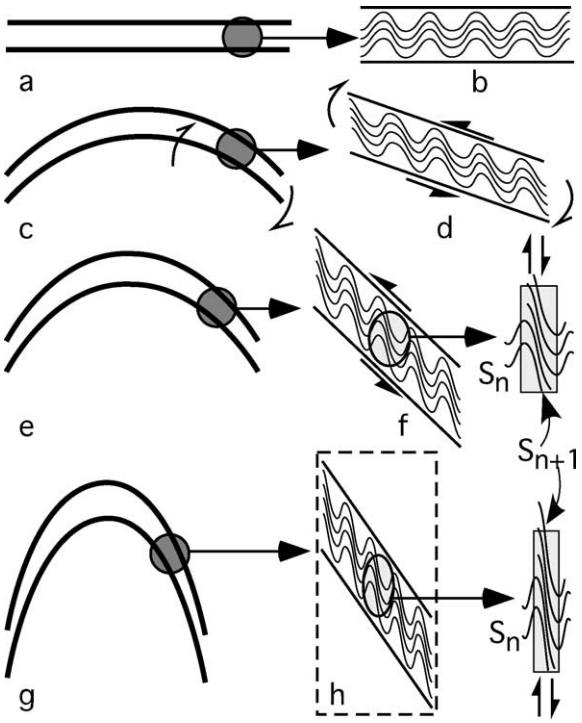

Fig. 1. Model of crenulation cleavage (S_{n+1}) development during folding by buckling. In this example fine-scale crenulations of S_n (subparallel to S_0) form by buckling due to bulk shortening ((a)–(c)), cleavage development (S_{n+1}) occurs through 'pressure solution' of long limbs ((f) and (h)), and the geometry of the cleavage orientation is a function of the competition between buckling rotation of the fold limbs S_0 ((c) and (e)) vs. shear on the folded foliation by flexural flow ((f) and (h)). Any shear on the cleavage S_{n+1} ((f) and (h)) only occurs late in the development of the fold.

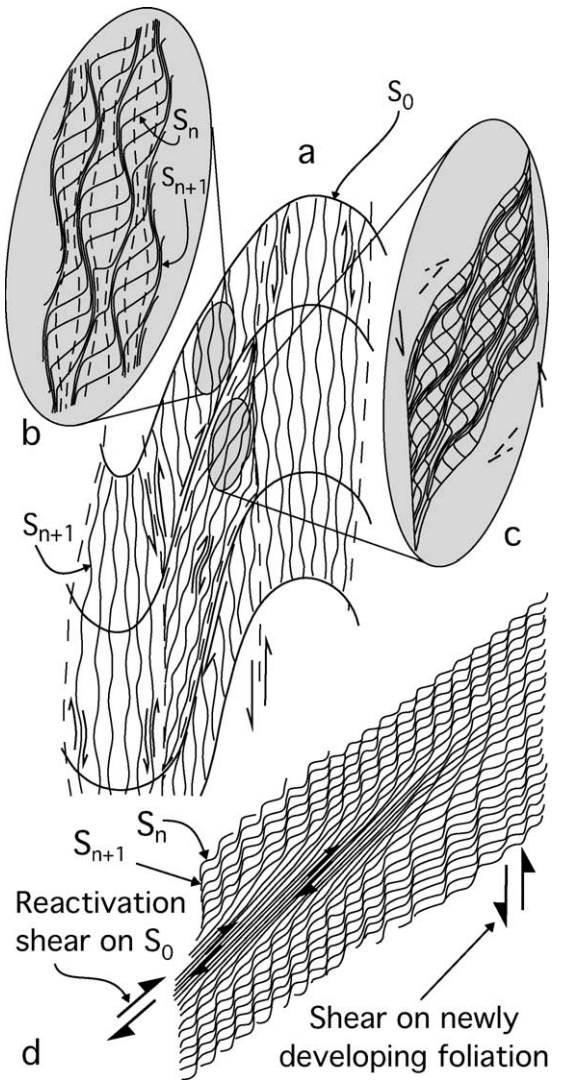

Fig. 2. Model of folding by progressive bulk inhomogeneous shortening after Bell (1981). The fold develops by partitioning of the deformation into zones of progressive shearing that (a) anastomose around zones of progressive shortening, and (b) sub-parallel to the axial plane and orthogonal to the direction of bulk shortening. The zones of progressive shearing (b) become differentiated crenulation cleavage seams (S_{n+1}) through shear strain controlled dissolution (Bell and Hayward, 1991). With continued shortening or, if a fold limb (S_0) is already present, reactivation of the fold limb occurs ((a) and (c)). Layer parallel shear during reactivation is antithetic relative to shear on the newly developing cleavage (S_{n+1}; (a) and (c)) and the deformation can switch backwards and forwards from axial plane shear (along S_{n+1}) to limb parallel shear (along S_0) at any scale along the one limb (a). Reactivation results in decrenulation and rotation of the crenulated cleavage S_n into parallelism with compositional layering S_0 on the fold limb (d).

shortening lying sub-parallel to the axial plane (Fig. 2b). As the fold limbs develop (Fig. 2a), deformation is commonly also partitioned into portions of the folded layers with an antithetic shear sense for the non-coaxial component of this deformation relative to the bulk rotation of the developing fold limb with respect to the axial plane (CW in Fig. 2c). This process, called reactivation, decrenulates newly formed crenulations of S_n (Fig. 2d) and may account for much of the progressive strain during deformation (Bell, 1986).

The significant difference between these two kinetic mechanisms is that during reactivation, at any scale along the fold limb, antithetic shear along the layering can stop and switch to synthetic shear parallel to the axial plane. This is not possible for flexural flow folding. The principal is shown at one scale in Fig. 2a (e.g. Bell et al., 2003). Detailed microstructural analysis of porphyroblasts using foliation inflexion/intersection lineations preserved within porphyroblasts (FIAs) and the overprinting asymmetry of inclusion and matrix foliations, should enable resolution of which of these mechanisms has occurred. We demonstrate this using rocks from the Appalachians in Vermont, where matrix foliations and bedding are sub-parallel and a famous series of domes are present. The Pomfret dome, lying north of the classic Chester dome (Fig. 3), provides an excellent area to study the relationship between foliations found within porphyroblasts, the matrix and macroscale folds. Microstructural evidence from porphyroblasts and the matrix reveals that the dome experienced a prolonged history of deformation, forming as an upright fold that predated porphyroblast growth, with strain accumulating progressively over many different events and deformation mainly being accommodated by foliation reactivation (e.g. Fig. 2a, c and d).

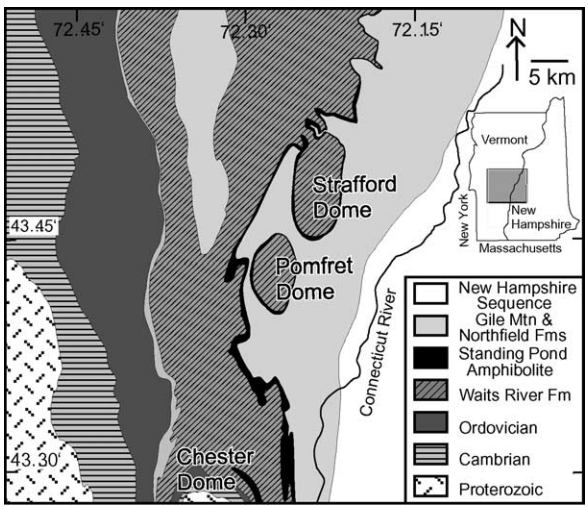

Fig. 3. Simplified geological map of central eastern Vermont (after Doll et al., 1961).

2. Geological setting

The Pomfret dome lies along the Chester–Strafford line of domes (Fig. 3; Osberg et al., 1989). The rocks affected by this dome are the mixed pelitic and quartzose Gile Mountain Formation and the underlying calcareous Waits River Formation. These rocks are potentially Silurian–Early Devonian in age (Hueber et al., 1990; Armstrong et al., 1997) and were deposited in the Connecticut Valley trough, an elongate, post-Taconic basin in which rapid and complex subsidence was localized during the Silurian, but affected the entire belt during the early Devonian (Bradley, 1983). Closure of the Connecticut Valley trough occurred during the Acadian orogeny (Bradley, 1983; Armstrong et al., 1992). Lyons (1955), the only person to have done detailed work previously around the Pomfret dome, believed that it formed late in the Acadian, and proposed that after initial upright folding, doming resulted from up-welling of an intrusive body that has not been exposed.

3. Mesoscopic to microscopic structure

S_1 has only been observed as inclusion trails in porphyroblasts. Intense matrix cleavage development (S_m), tight to isoclinal folding of compositional layering, and the lack of younging indicators, made it difficult to trace bedding (S_0) across many outcrops. S_0 is sub-parallel to S_m.

S_2 is an intense bedding-parallel foliation that is folded around D_3 folds (Fig. 4a) but has only been seen mescoscopically at location 79 (Figs. 4a and 5), where a D_3 fold of S_2 has been refolded by a D_4 fold, and at Location 149 (2.5 km east of the map edge in Fig. 5 along Route 14) where interbedded psammites and quartzites preserve S_2 to S_5. S_2 is seen rarely (Fig. 4c) in porphyroblast strain shadows and is generally parallel to S_0. No D_2 folds of S_0 were found.

Rare near isoclinal D_3 folds with upright axial planes have been asymmetrically refolded by D_4 (Fig. 4a). S_3, a penetrative differentiated foliation, is crenulated or rotated by D_4 and generally preserved as a bedding-parallel foliation. In areas of low D_4 strain adjacent to porphyroblasts, S_3 has a sub-vertical orientation and S_2 is locally preserved at a high angle to it (Fig. 4c).

D_4 produced folds that are typically tight to isoclinal, but generally only preserved in some layers (Fig. 4). Shallowly plunging D_4 fold axes in the centre of the dome steepen towards its margins (Fig. 5c). Large (10 m) D_4 folds (sample locality AV32, Fig. 5a) near the dome hinge are generally symmetric, with smaller parasitic folds on their limbs. S_4 is a differentiated crenulation cleavage heterogeneously developed to stages 3, 4 and, locally, 6 of Bell and Rubenach's (1983) classification. S_4 dips gently and is sub-horizontal adjacent to porphyroblasts or in zones of low D_5 strain (Figs. 5a and 6b). With increasing D_5 intensity away from the dome hinge, a composite

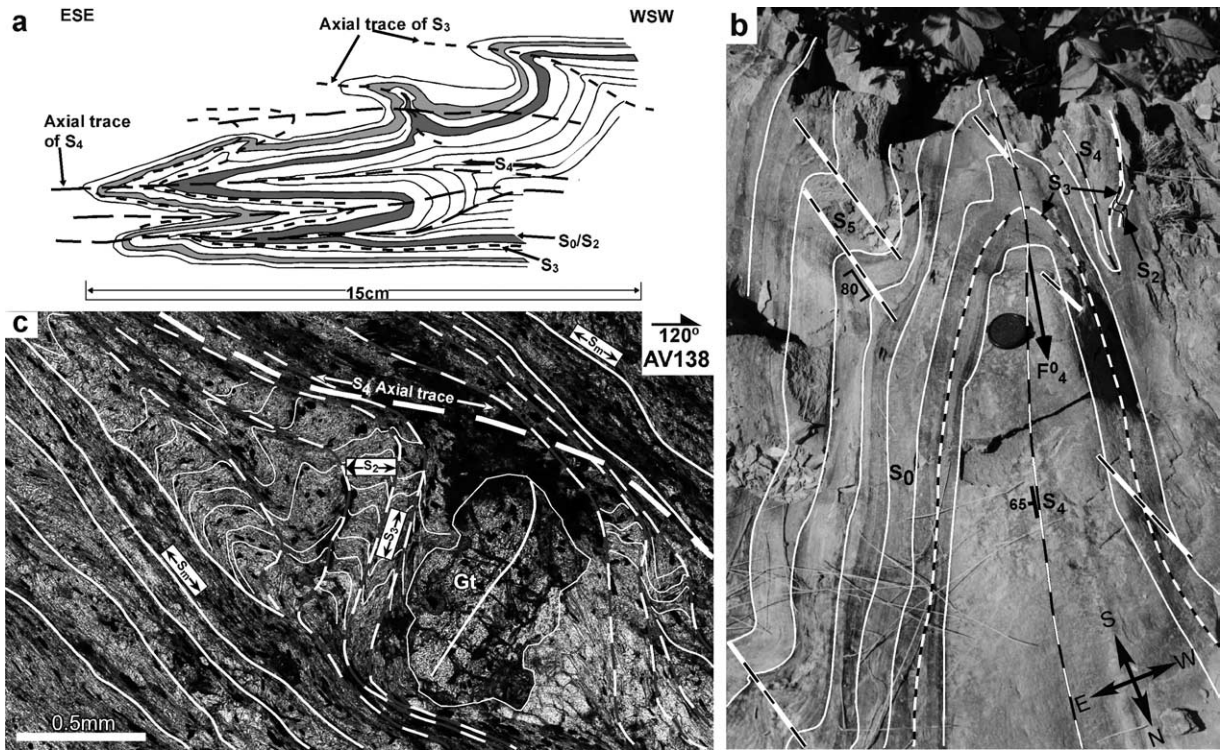

Fig. 4. (a) Early upright D_3 fold of S_0//S_2 refolded during D_4 (location 79; Fig. 5). S_3, rotated from a steep to gently dipping with an overall ACW asymmetry during D_4, occurs as a fully differentiated and penetrative fabric that is preserved parallel to S_0 after the effects of D_4 and D_5. (b) Isoclinal D_4 fold (road outcrop, location 149, 0.9 km west of Hartford on Route 14). D_5 heterogeneously overprints D_4 with an east side up differentiation asymmetry rotating the S_4 axial plane to a steep inclination. In the upper right corner S_3 overprints S_2. Plan view looking SSW. D_4 fold plunges 58° → 012°. (c) S_2, preserved adjacent to a garnet porphyroblast on east limb of the Pomfret dome, is sub-horizontal in the microlithons of a steep differentiated S_3. Sub-horizontal foliation S_4, crenulates and rotates S_3 and unfolds S_2. Away from the porphyroblast, reactivation of S_3 destroys remains of S_2 and forms a strong foliation S_m parallel to S_0. Vertical thin section. Single barbed arrow indicates way up and strike. Sample AV138.

foliation called S_m, due to the effects of D_2–D_4, lies parallel to S_0 (Figs. 4, 5 and 6c and d). S_m is the foliation mapped by White and Jahns (1950) and Lyons (1955) as being domed with S_0 (Fig. 5).

D_5 folds and crenulations with steeply dipping, NNE-striking, axial planes (Figs. 4 and 5) progressively rotate and tighten D_4 folds outward from the dome core (Fig. 5) until S_4 cannot be distinguished from S_5. S_5 is most intensely developed adjacent to heterogeneities, and locally forms a differentiated crenulation cleavage (Fig. 6), but is poorly developed in the dome core. The D_5 crenulation asymmetry switches from ACW to CW from the west to east side of the dome (Fig. 7). $L^0_{4,5}$ intersection lineations plunge N to NE at the north end of the dome and S to SW at the south end (Fig. 5c and d). D_5 superficially appears to be the event that formed the dome.

D_6 folds of both bedding and S_5 have axial planes that are sub-horizontal, but this event only forms very locally. Microscopically, D_6 occurs as a stage 2 crenulation or local kinks of S_5. S_m occurs as a schistosity parallel to compositional layering. This foliation appears to have resulted from the cumulative effects of a number of deformations. Only where S_4 was measured in D_5 low strain zones is it referred to on the map as S_4 (Fig. 5b).

4. Foliations preserved within porphyroblasts

4.1. Foliation intersection/inflection axes (FIAs) and their determination

FIAs are measured for a sample, independent of assumptions concerning timing inclusion trails relative to matrix structures and whether or not the porphyroblasts have rotated, using geographic coordinates and the vertical as a reference frame (Hayward, 1990; Bell et al., 1995). Up to 18 vertical thin sections striking every 10° from 0 to 170° were cut from each spatially oriented sample (Table 1). The FIA trend is located where the asymmetry of inclusion trails switches between successive vertical sections around the compass when viewed in one direction (e.g. Bell et al., 1995, 1998, 2003). The inclusion trails in most samples collected around the Pomfret dome are truncated by S_m (Fig. 8). However, in some they are continuous with the matrix foliation (Fig. 9).

4.2. FIA analysis of garnet porphyroblasts within and around Pomfret dome

Sixty-seven FIAs were measured from garnet porphyroblasts within 41 spatially oriented samples (Table 1; Fig. 10).

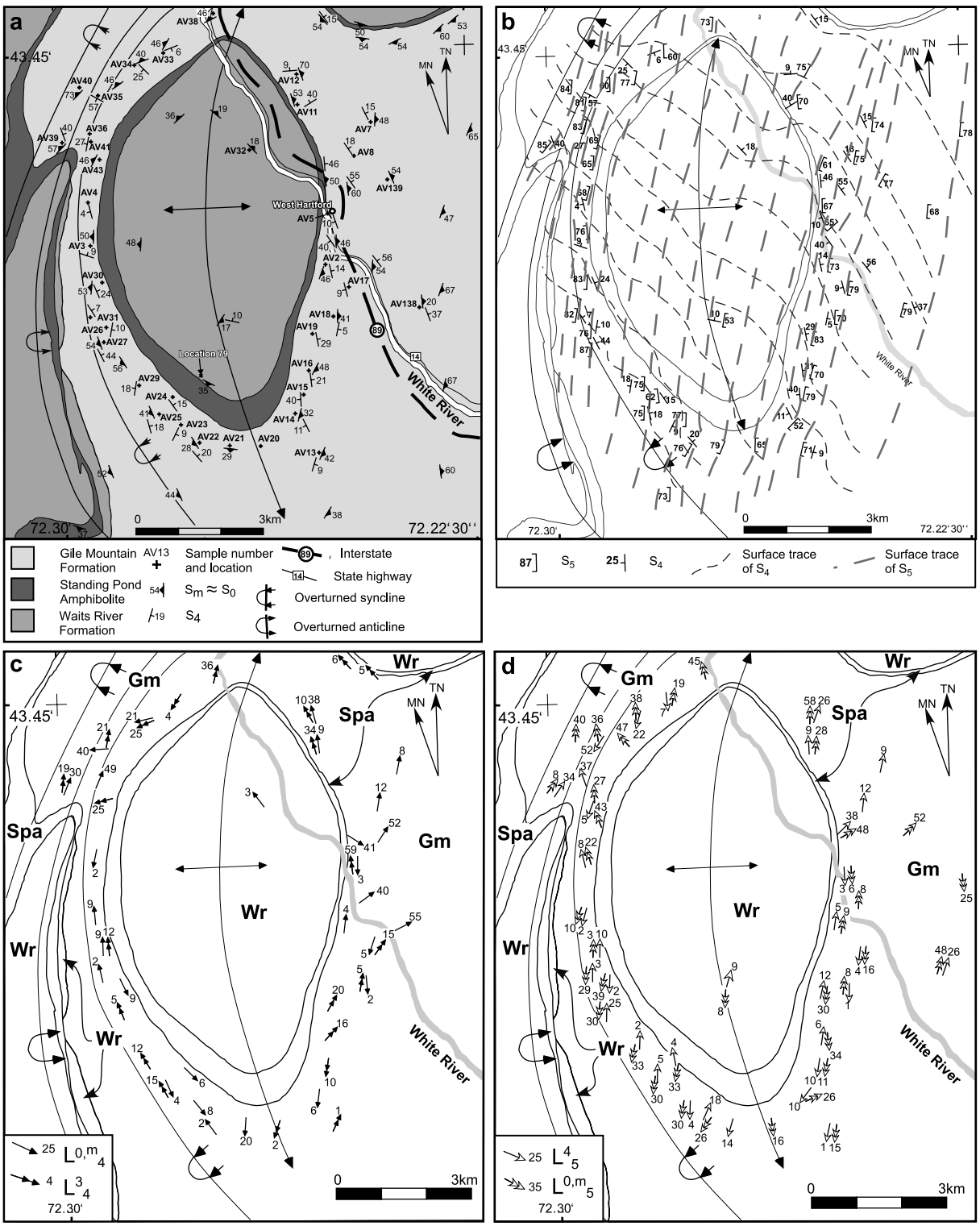

Fig. 5. (a) Simplified geological map of the Pomfret dome area showing S_m (bedding parallel foliation representing a composite foliation resulting from the effects of at least D_3, D_4 and D_5), and S_4 together with the sample localities used for this study. S_m dips in a radial fashion from the dome core. Locations 79 and 149 (2.5 km east of map edge along Route 14) are sites where rare mesoscopic D_3 folds are preserved (see Fig. 4). (b) Structural map showing S_4 and S_5 and their trend surfaces. S_4 has an overall NW trend and S_5 maintains a consistent N–NNE trend. (c) Structural map showing intersection lineations $L_4^{0,m}$ and L_4^3. (d) Structural map showing intersection lineations $L_5^{0,m}$ and L_5^4. Note the general switch in plunge from north to south of the dome for both $L_4^{0,m}$ and $L_5^{0,m}$.

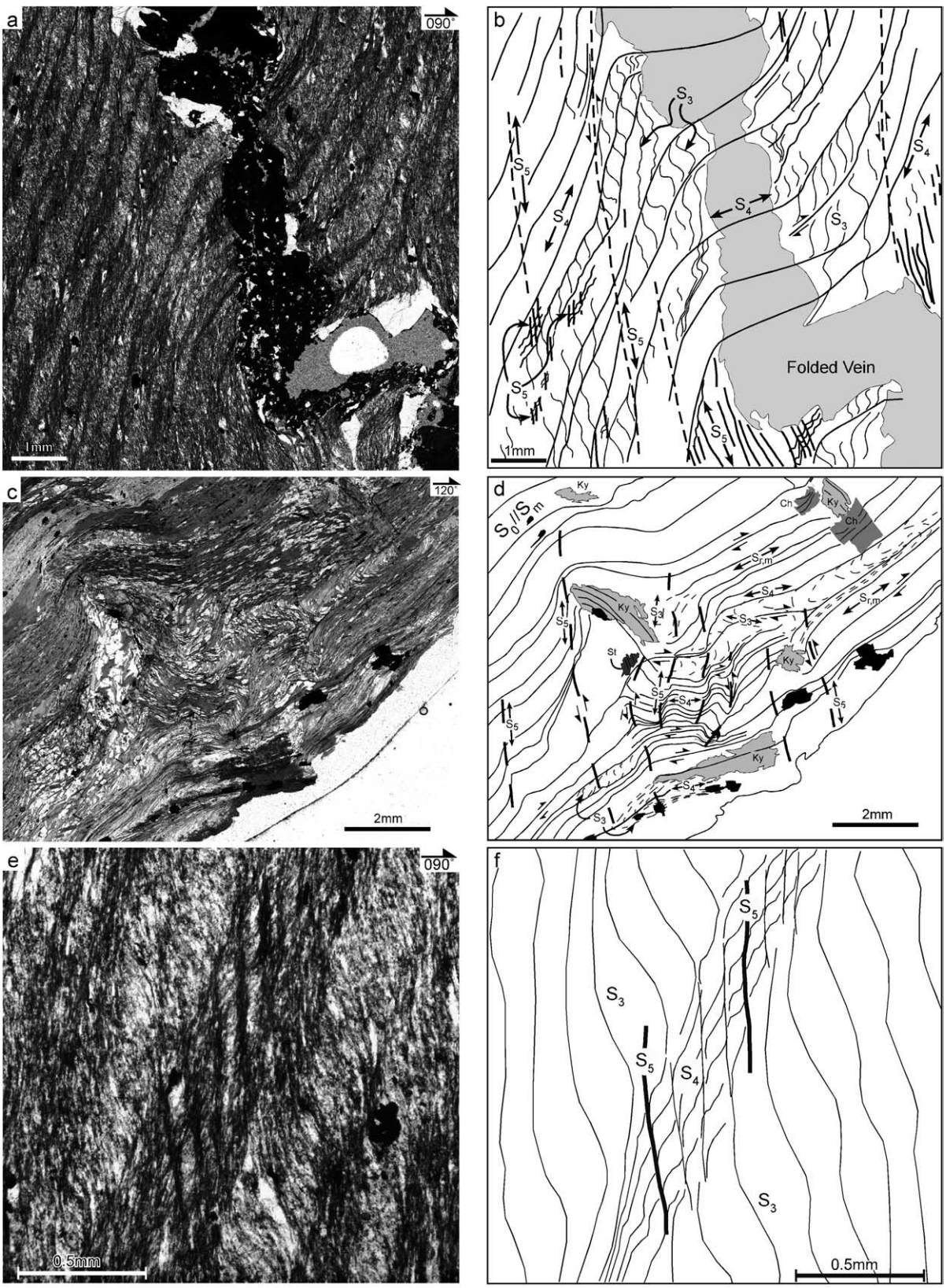

Fig. 6. ((a) and (b)) Vein subparallel to S_3, cut by S_4 and overprinted by S_5. The original sub-vertical and sub-horizontal nature of S_3 and S_4 are preserved. Shear sense on S_4 is top to the east. S_5, obvious in the P domains of S_4 (see e,f), pitches steeply east. Shear sense of S_5 on S_4 is east side up. Sample AV132. Plane polarized light. ((c) and (d)) Heterogeneous, weakly developed sub-vertical S_5 overprints sub-horizontal S_4 on the west limb of the Pomfret dome. S_4 crenulates S_3, which is sub-vertical adjacent to kyanite (Ky) and staurolite porphyroblasts (St). Away from the porphyroblasts, S_4, reactivated during D_5, has decrenulated and unfolded D_5 crenulations. Reactivated foliations labelled $S_{r,m}$ and the sense of shear on the reactivated layer is antithetic to shear on S_5. $S_0//S_m$. Sample AV30. ((e) and (f)) Detail of (a) reveal asymmetry of S_4 on S_3 and S_5 on S_4. All sections vertical with single barb showing way up. Plane polarized light.

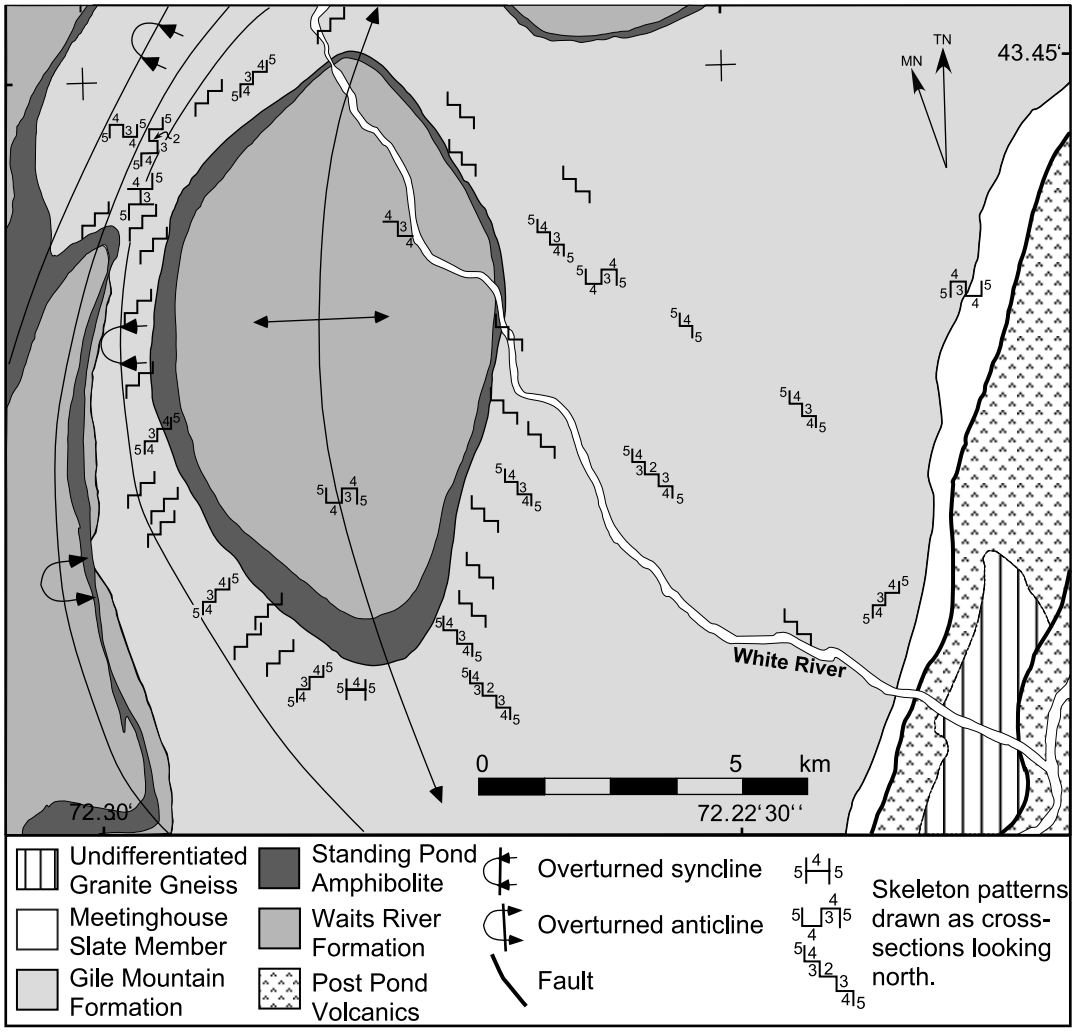

Fig. 7. Map of the asymmetry of successive matrix foliations represented as skeletal patterns, drawn as cross-sections looking north in west–east striking vertical thin sections (i.e. orthogonal to the regional strike of S_5). A distinct staircase geometry dominates both limbs of the Pomfret dome with the D_5 crenulation asymmetry switching from CW (i.e. west side up) looking north on the eastern side of the dome, to ACW (i.e. east side up) on the western side of the dome. On the eastern limb of the dome, the asymmetry of S_4 on S_3 is dominated by ACW (i.e. top to the west shear) and CW (i.e. top to the east shear) on the western limb.

Sixteen samples contain a different FIA in the core vs. the rim, and five contain a different FIA in the core vs. the median vs. the rim (Tables 1 and 2). Some of the FIAs determined were from crenulations incorporated during the development of a younger crenulation event at the time of garnet growth (called pre-porphyroblast crenulation FIAs; Table 1). Six FIAs were measured using kyanite and staurolite porphyroblasts (Table 1). The total plot of garnet FIAs shows five clusters of trends oriented NW–SE, NE–SW, E–W, NNW–SSE, and NNE–SSW (Fig. 10a). The same five clusters of trends are also visible in the multiple FIA plots (Fig. 10b). The rose plot of single FIAs shows only four of these maxima (Fig. 10c). The NNW–SSE one is missing.

4.3. Relative timing from multi-FIA samples

A FIA trend determined from the core of the porphyroblast must be older than a FIA from the rim for the same sample (Table 2; Fig. 8). If a consistent succession of trends relative to timing is present, a paragenesis of trends for multiple FIA samples can be determined (e.g. Bell et al., 1998). The following relationships were observed from sample to sample in garnet porphyroblasts:

1. NW–SE-trending FIAs in cores, succeeded by SW–NE, W–E, NNW–SSE or SSW–NNE FIAs in the medians or rims (Table 2). Where the only FIA present is NW–SE, the inclusion trails are truncated by the matrix foliation (Table 2).
2. SW–NE-trending FIAs in cores succeeded by W–E or NNW–SSE FIAs in the rims (Table 2). Sample AV17b contains a NW–SE core FIA, a SW–NE rim FIA in garnet and a SSW–NNE FIA in staurolite and kyanite porphyroblasts (Table 2). Sample AV13 contains a FIA-trending SW–NE in garnet but younger staurolite porphyroblasts contain a FIA-trending SSW–NNE.

Table 1
Samples collected from around the Pomfret dome (shown in Fig. 5), the geological formations from which they were taken, latitude and longitude, FIA trend, strikes of vertical thin sections cut for FIA determination, and horizontal (Hz) thin sections used. Gm = Gile Mountain Formation; Wr = Waits River formation

Sample	Location		Fmn	FIA trend—garnet				St	Ky	Strike of vertical thin sections used relative to true north																		
	Longitude	Latitude		PPC	Core	Med	Rim																					
East limb																												
AV2	72.4196	43.7021	Gm		120		85			0	30	40	50	60	70	80	90	100	110	120	130	140	150	Hz				
AV5a	72.4166	43.7133	Gm		135	55	175			0	20	30	40	50	60	70	80	90	100	110	120	130	140	150	160	170	Hz	
AV5b	72.4166	43.7133	Gm		135	45	175	10		0	20	30	40	50	60	70	90	100	110	120	130	140	150	160	170	Hz		
AV7	72.4042	43.7332	Gm		50					0	30	40	50	60	70	80	90	120	150	Hz								
AV8	72.4096	43.7259	Gm		60					0	30	50	60	70	80	90	120	150	Hz									
AV11	72.4267	43.7375	Gm		100		25			0	20	30	40	60	80	90	100	120	150	Hz								
AV12	72.4263	43.7445	Gm		140		30			0	5	10	20	20	30	60	70	90	110	120	130	140	145	150	160	170	Hz	
AV13	72.4212	43.6604	Gm		50		55	25		0	10	20	30	40	50	60	60	90	90	120	150	170	Hz					
AV14	72.4298	43.6691	Gm		45					0	30	40	50	60	90	120	150	Hz										
AV15	72.4270	43.6736	Gm		125	45	85			0	10	20	30	50	60	70	80	90	120	130	140	150	160	170	Hz			
AV16b	72.4258	43.6787	Gm		120		165			0	10	30	60	90	120	130	140	150	160	170	Hz							
AV17b	72.4125	43.6971	Gm		130	60	55	15	15	0	10	20	30	40	50	60	70	80	90	100	110	120	130	140	150	160	170	Hz
AV18	72.4172	43.6906	Gm		135		95			0	10	30	40	50	60	70	80	90	100	110	120	130	140	150	160	Hz		
AV19	72.4238	43.6868	Gm		55		90			0	10	20	30	40	50	60	70	80	90	100	110	120	130	140	150	160	170	Hz
AV20	72.4412	43.6624	Gm		60		150			0	30	50	60	70	90	120	140	150	150	Hz								
AV32b	72.4416	43.7278	Wr		25					0	10	20	30	40	60	90	120	150										
AV138	72.3914	43.6918	Gm		10					0	20	30	60	90	120	130	140	150	160	160	170	Hz						
AV139	72.3996	43.7205	Gm		125*					0	10	30	60	90	100	120	130	140	150	160	170	Hz						
West limb																												
AV3	72.4911	43.7075	Gm		110					0	30	50	60	70	80	90	110	110	120	130	140	150	160	170	Hz			
AV4	72.4912	43.7173	Gm		100		15			0	30	60	70	80	90	100	110	120	150	Hz								
AV21	72.4501	43.6628	Gm		35					0	30	40	50	60	90	110	120	130	140	150	150	150	Hz					
AV22	72.4593	43.6633	Gm		50	160	165			0	30	40	50	60	90	120	130	140	150	160	170	Hz						
AV23	72.4647	43.6676	Gm		45		160			0	10	30	40	50	60	70	80	90	120	130	140	150	160	175	Hz			
AV24	72.4673	43.6738	Gm		135*					0	10	20	30	60	90	120	130	140	150	160	170	Hz						
AV25	72.4714	43.6698	Gm		135					0	10	30	60	90	110	120	130	140	160	170	Hz							
AV26a	72.4872	43.6895	Gm		85*					0	10	20	30	40	50	60	70	80	90	100	110	120	130	150	Hz			
AV27	72.4878	43.6864	Gm		15					0	10	20	30	40	60	90	120	120	130	150	160	170	Hz					
AV29	72.4776	43.6768	Gm		40*					0	10	20	30	40	50	60	70	80	90	100	120	150	170	Hz				
AV30	72.4877	43.6994	Gm	135			155	10	10	20	50	70	80	100	110	120	130	140	150	160	170	180	Hz					
AV31	72.4916	43.6920	Gm	45			95		15	0	10	20	30	40	50	60	70	80	90	100	120	130	140	150	160	170	Hz	
AV33	72.4672	43.7500	Gm		85		155			0	10	20	30	40	50	60	70	80	90	100	110	120	130	140	150	160	170	
AV34	72.4759	43.7473	Gm		130					0	30	60	90	110	120	130	140	150	160									
AV35	72.4871	43.7408	Gm		135					0	0	30	30	60	90	130	140	150	160	170	Hz							
AV36c	72.4900	43.7324	Wr?		120		15			0	30	60	90	100	110	120	130	140	150	Hz								
AV36v	72.4900	43.7324	Wr?		125		75			0	30	60	70	80	90	100	110	120	130	140	150	160	170	Hz				
AV36z	72.4900	43.7324	Wr?		125		80			0	30	60	70	90	100	110	120	130	140	150	Hz							
AV38	72.4512	43.7583	Gm		130					0	30	60	90	110	120	130	140	150	160	Hz								
AV39	72.4986	43.7306	Gm		135			20	20	0	0	10	30	60	90	110	110	120	130	140	150	160	170	170	Hz			
AV40	72.4927	43.7428	Gm		125					0	30	60	90	110	120	130	140	150	160	Hz								
AV41	72.4896	43.7306	Gm		20					0	10	20	30	60	90	120	130	140	150	160	170							
AV43	72.4870	43.7268	Gm		40					0	10	20	30	40	50	60	90	100	110	120	130	140	150					

Table 2
Shows relative succession of FIAs for samples containing more than one FIA. Separated according to which FIA trend came first and east vs. west limbs of the Pomfret dome

Sample	Garnet FIA trend			
	PPC	Core	Median	Rim
East limb				
AV2		120		85
AV5a		135	55	175
AV5b		135	45	175
AV12		140		30
AV15		125	45	85
AV16b		120		165
AV17b		130	60	55
AV18		135		95
West limb				
AV30	135			155
AV36c		120		15
AV36v		125		75
AV36z		125		80
East Limb				
AV13		50		55
AV19		55		90
AV20		60		150
West Limb				
AV22		50	160	165
AV23		45		160
AV31	45			95
East Limb				
AV11		100		25
West Limb				
AV4		100		15
AV33		85		155

3. W–E-trending FIAs in cores succeeded by NNW–SSE or SSW–NNE FIAs in the rims (Table 2) or truncated by the matrix foliations.
4. SSW–NNE-trending FIAs (Tables 1 and 2) contain inclusion trails that are generally continuous with the matrix foliation.

The succession of FIAs suggested by this data is NW–SE, SW–NE, W–E, NNW–SSE, SSW–NNE. The youngest of these FIA sets trending SSW–NNE is the only one preserved within staurolite and kyanite porphyroblasts, which contain inclusions trails where S_i is continuous with S_e (Tables 1 and 2; Fig. 9c and d). Plagioclase and biotite (Fig. 9b) overgrow the matrix foliations and contain the intersection lineations L_5^0 and L_5^4 described above (Table 3).

5. Foliation asymmetry

5.1. Matrix foliation differentiation asymmetry

The differentiation asymmetry (Bell et al., 2003) or curvature of a crenulated cleavage into a differentiated crenulation cleavage seam, was determined looking north in W–E striking vertical thin sections. The asymmetry of S_4 into S_5 is CW on the east limb of the dome and ACW on the west limb (Figs. 4c, 7 and 8). The asymmetry of S_3 into S_4 is ACW on the east limb of the dome and CW on the west limb (Figs. 6a, b, e and f and 7). S_2 is too rarely preserved in the matrix to determine reliable asymmetries of S_2 into S_3. However, S_2, S_3 and S_4 are preserved in porphyroblasts where the trails are continuous with the matrix foliation and define the SSW–NNE-trending FIA set 4.

Table 3
Shows FIAs divided according to the succession of sets determined from the multi-FIA data shown in Table 2 and described in the text

Sample	Fmn	FIA sets—garnet					St	Ky
		Set 0	Set 1	Set 2	Set 3	Set 4	Set 4	
East limb								
AV2	Gm	120		85				
AV5a	Gm	135	55		175			
AV5b	Gm	135	45		175		10	
AV7	Gm		50					
AV8	Gm		60					
AV11	Gm			100		25		
AV12	Gm	140	30					
AV13	Gm		50 + 55				25	
AV14	Gm		45					
AV15	Gm	125	45	85				
AV16b	Gm	120			165			
AV17b	Gm	130	60 + 55				15	15
AV18	Gm	135		95				
AV19	Gm		55	90				
AV20	Gm		60		150			
AV32b	Wr					25		
AV138	Gm					10		
AV139	Gm	125						
West limb								
AV3	Gm			110				
AV4	Gm			100		15		
AV21	Gm		35					
AV22	Gm		50		160 + 165			
AV23	Gm		45		160			
AV24	Gm	135						
AV25	Gm	135						
AV26a	Gm			85				
AV27	Gm					15		
AV29	Gm		40*					
AV30	Gm	135			155		10	10
AV31	Gm		45	95				15
AV33	Gm			85	155			
AV34	Gm	130						
AV35	Gm	135						
AV36c	Wr?	120				15		
AV36v	Wr?	125		75				
AV36z	Wr?	125		80				
AV38	Gm	130						
AV39	Gm	135					20	20
AV40	Gm	125						
AV41	Gm					20		
AV43	Gm		40					
Average FIA		130	48	90	162	18	16	15

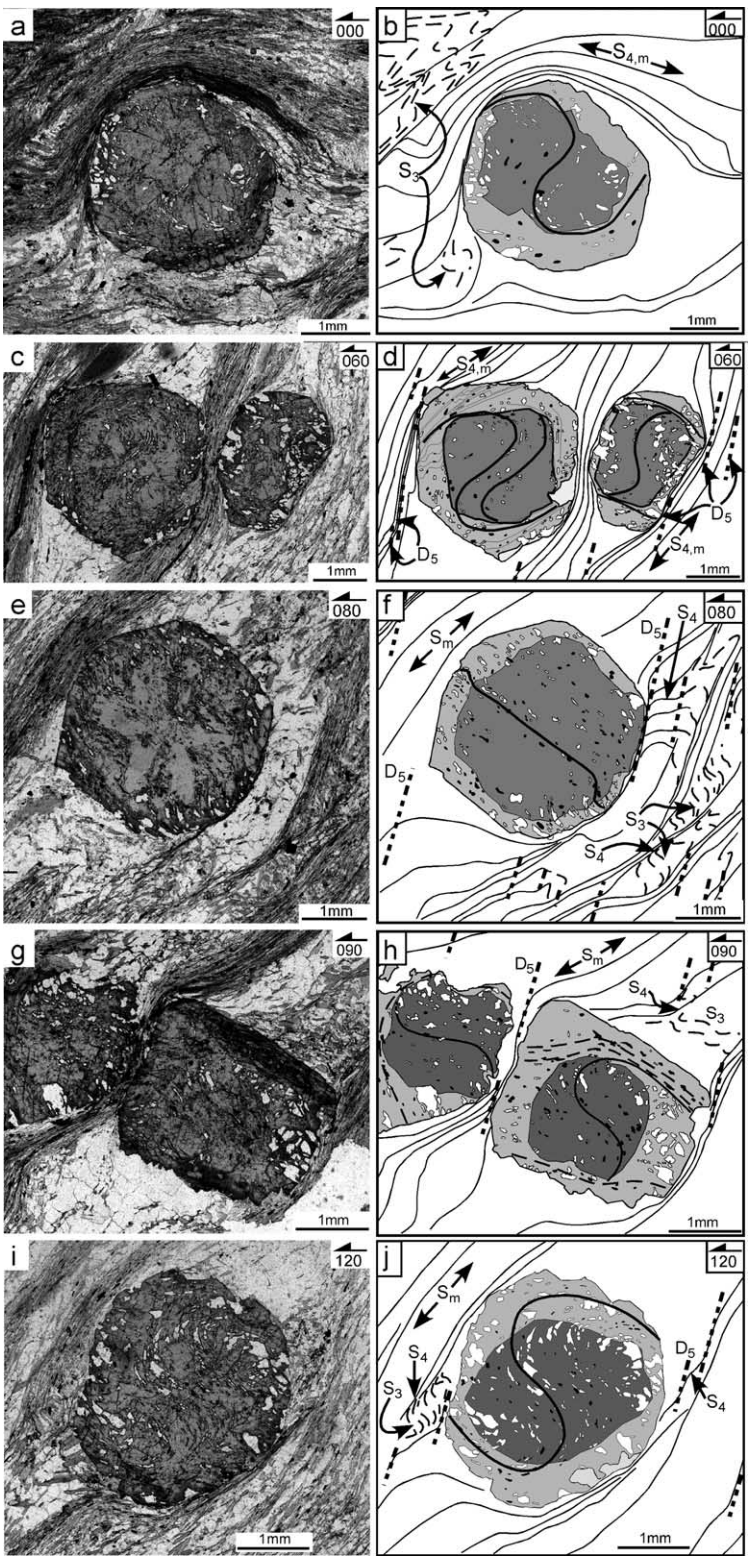

Fig. 8. Asymmetry method to determine the FIA in sample AV19 from the east limb of the Pomfret dome. ((a) and (b)) Garnet porphyroblast with ACW shaped spiral inclusion trail—vertical section striking 000°. ((c) and (d)) Garnet porphyroblasts with opposite asymmetries in the core but ACW asymmetries in the rim—vertical section striking 060°. ((e) and (f)) Garnet porphyroblast with CW trails in the core and ACW ones in the rim—vertical section striking 080°. ((g) and (h)) Garnet porphyroblasts with CW asymmetries in the core and the rim—vertical section striking 090°. ((i) and (j)) Garnet porphyroblast with CW asymmetry in the core and rim—vertical section striking 120°. Core FIA at 060°. Rim FIA at 085°. N.B. c-j look approximately south rather than north.

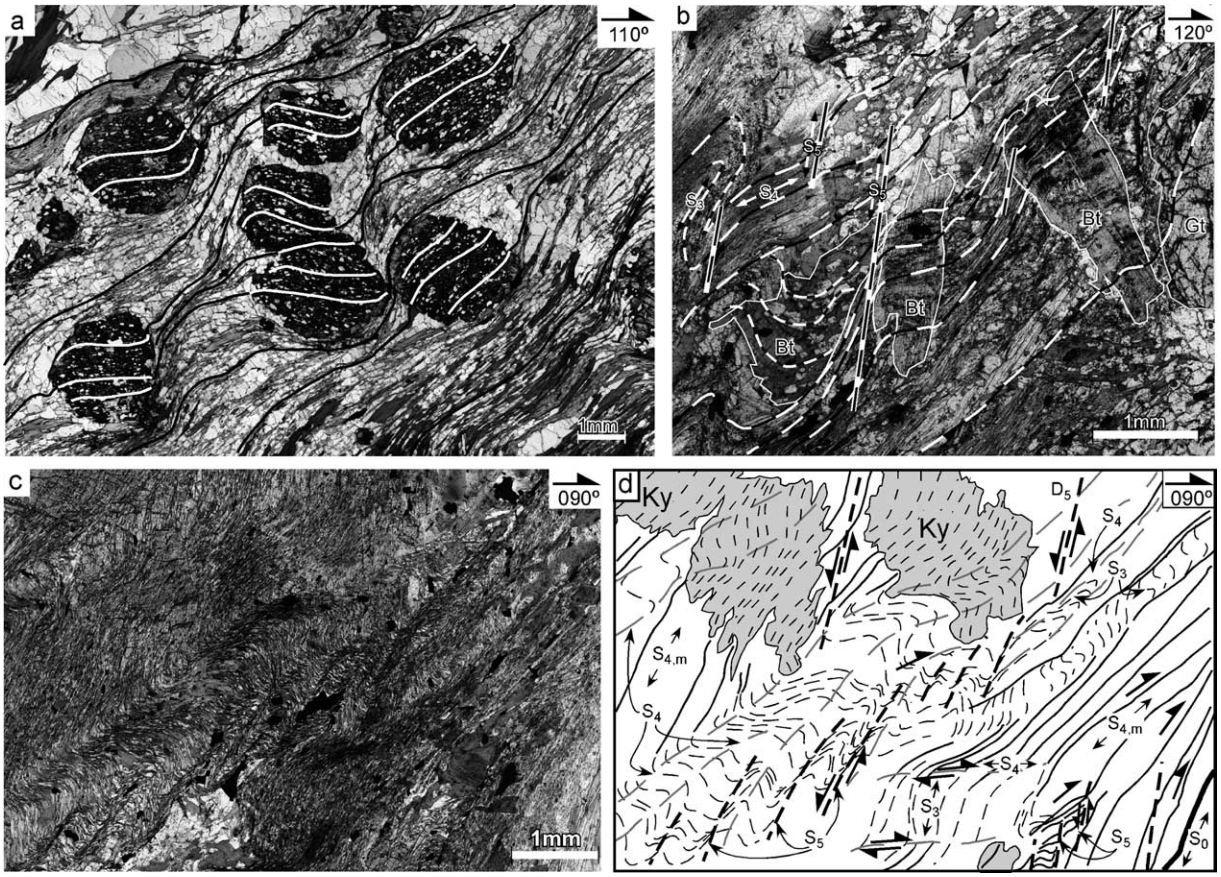

Fig. 9. (a) Garnet porphyroblasts with the trails continuous with the matrix foliation. Garnet grew during D_5. S_5 between the porphyroblasts is a steeply pitching differentiated crenulation cleavage. Sample AV27, west limb of the Pomfret dome. (b) Biotite porphyroblasts with trails continuous with the matrix foliation. Biotite grew early in D_5. Sample AV36c, west limb of the Pomfret dome. Vertical thin section. ((c) and (d)) Kyanite porphyroblasts in sample AV39, west limb of the Pomfret dome. Kyanite grew in both D_4 and D_5. Other porphyroblasts grew only syn-D_5. Reactivation during D_5 parallel to S_4 unfolded D_4 crenulations of S_3 (e.g. Bell, 1986) and locally rotated S_3 towards parallelism with S_5. S_5 is in turn rotated towards parallelism with S_4 by reactivation of S_4. All thin sections are vertical, the light is plane polarised and the single barbed arrow indicates way up and strike.

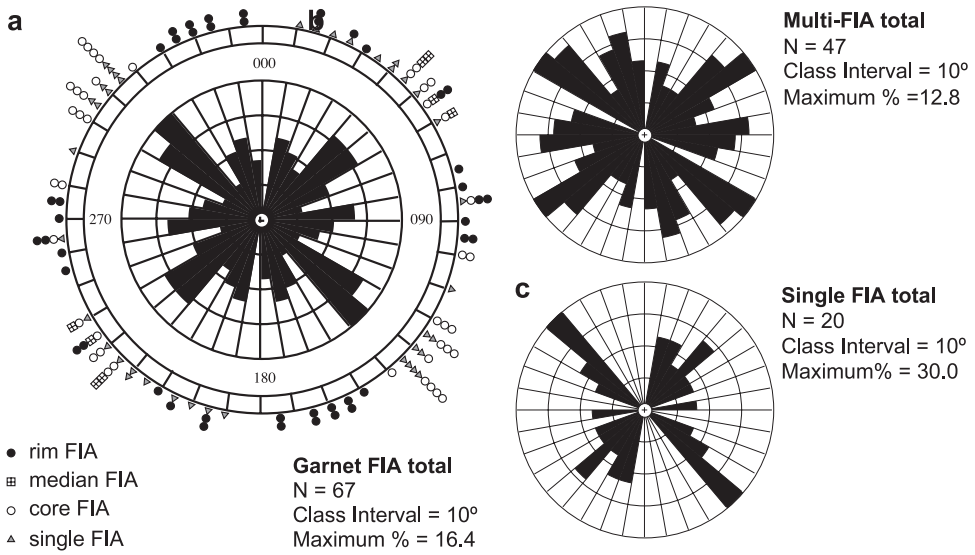

Fig. 10. (a) Plot of the total garnet FIA trends for the samples collected around the Pomfret dome. Inner plot is a true area rose diagram (radii = square root of frequency). Outer plot shows raw FIA trends of the single FIA samples and the core, median and rim FIAs from multi-FIA samples. (b) True area rose plot of the total Multi-FIAs for the Pomfret dome. Five distinct maxima are clearly seen oriented NW–SE, NE–SW, E–W, NNW–SSE and NNE–SSW. Single FIA data plotted in (c) show only four maxima, NW–SE, NE–SW, E–W and NNE–SSW.

5.2. Foliation asymmetry preserved within porphyroblasts

The CW or ACW asymmetry of successive overprinted foliations within porphyroblasts directly reflects the differentiation asymmetry for each overprinting event (Bell et al., 2003). The asymmetries defining NW–SE-trending FIAs called set 0 (see below) were determined from vertical thin sections near orthogonal to this trend looking NW. Those for sets 1–4 were determined looking NE, E, NNW, and NNE, respectively. Fig. 11a shows a histogram in which each sample appears once depending on whether the asymmetries are CW, ACW or both are represented, separated according to FIA set and dome limb. Fig. 11b shows histograms where only each flat to steep succession of overprinted foliations (shown on the fold inset) preserved within a sample is plotted separated according to FIA set and dome limb. Fig. 11c shows a histogram where each sample appears once according to whether the inclusion trail asymmetries are predominantly CW or ACW for FIA set 2. The data is separated based on whether the sample lies in the northern or southern half of the Pomfret dome across a W–E-trending axial plane to test whether this nearly circular but slightly N–S elongated dome formed originally as a slightly W–E elongated dome.

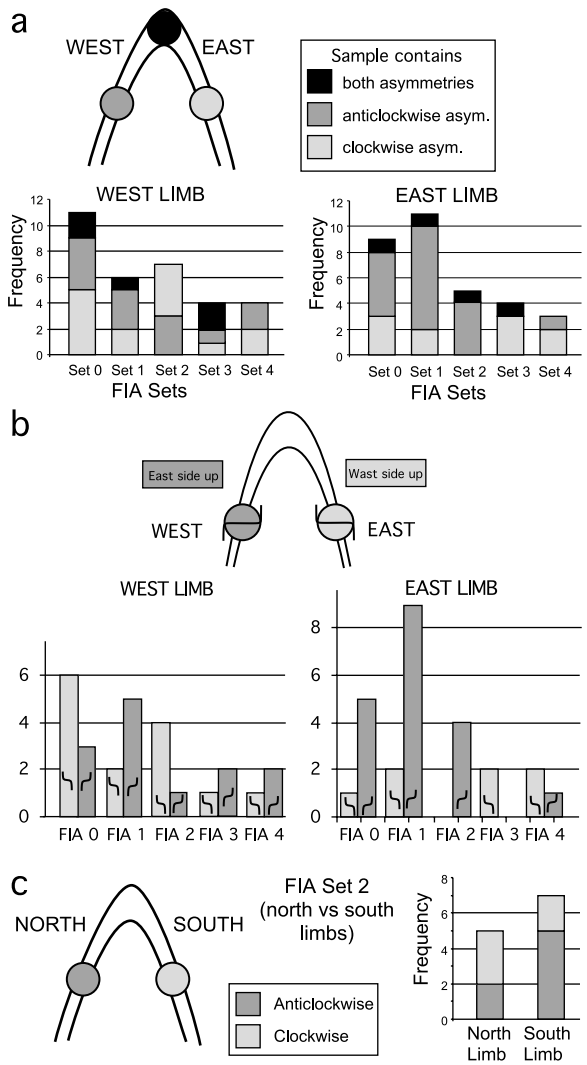

Fig. 11. Histograms showing the inclusion trail asymmetries for the succession of five FIA sets recorded herein separated according to which limb of the Pomfret dome the samples lie on. (a) Shows total asymmetries recorded as CW or ACW on either limb. (b) Shows asymmetries for foliations shifting from flat to steep orientations. The asymmetries for FIA set 2 are shown looking east. (c) Shows the asymmetries for the W–E-trending FIA set 2 separated according to whether the sample lies in the northern half vs. the southern half of the dome to test for an initially W–E-trending regional fold geometry.

6. Comparison of FIA trends across the Pomfret dome

The rose diagram of total garnet FIAs (Fig. 10) contains five clusters of trends trending NW–SE, SW–NE, E–W, NNW–SSE and SSW–NNE. Separating this data into the west (Fig. 12a) and east (Fig. 12f) limbs (Table 2) shows the same five distinct clusters of FIA trends on each, although the relative proportions vary. Samples containing a sequence of FIAs from core to rim reveal a consistent succession of peaks from NW–SE, SW–NE, E–W, NNW–SSE to SSW–NNE. Separating this FIA data into the west (Fig. 12d) and east (Fig. 12f) limbs, shows that the NNE–SSW-trending cluster peak is missing from the east limb although it is present in the single FIA data that is included in Fig. 12c. The five successive sets of FIAs are shown in plan view in Fig. 13 for all measured data.

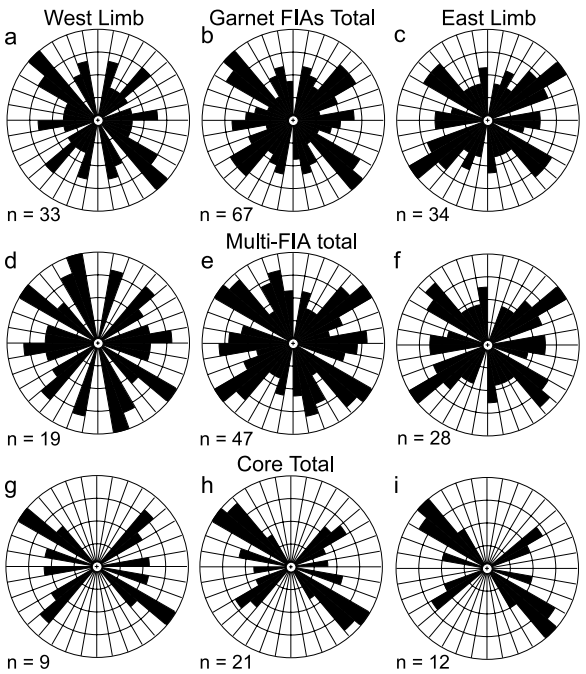

Fig. 12. Series of rose diagrams showing the various FIAs on each limb of the Pomfret dome as well as the two limbs combined. Total garnet FIAs for the west limb (a), combined limbs (b) and east limb (c). Multi FIAs for the west limb (d), combined limbs (e) and east limb (f). Core FIAs for the west limb (g), combined limbs (h) and east limb (i).

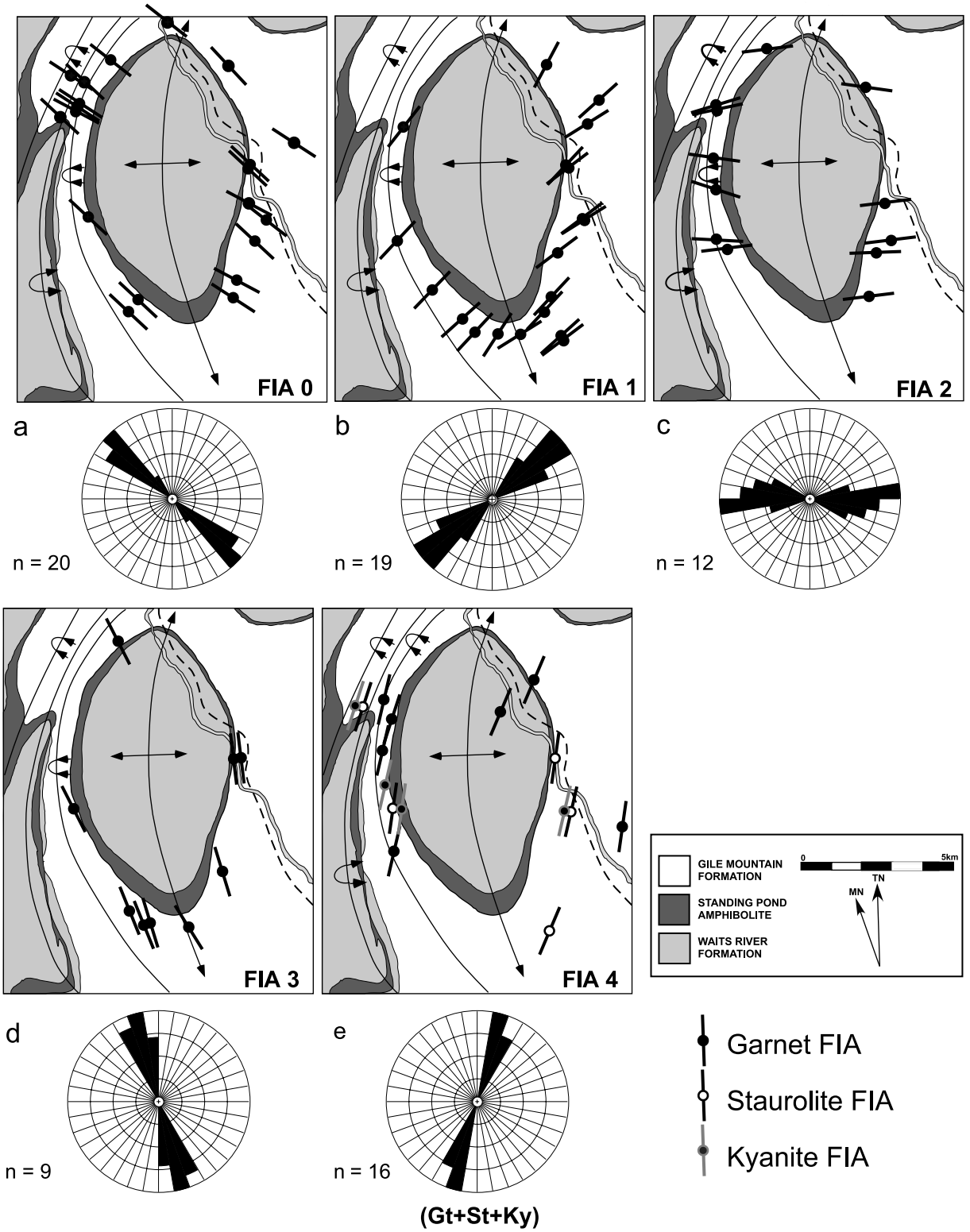

Fig. 13. FIA trends for successive FIA sets in the Pomfret dome area. (a) Map and rose diagram of FIA set 0 trends for the samples collected around the Pomfret dome. (b) Map and rose diagram of FIA set 1 trends for the samples taken from the same area as (a). (c) Map and rose diagram of FIA set 2 trends for the samples taken from the same area as (a). (d) Map and rose diagram of FIA set 3 trends for the samples taken from the same area as (a). (e) Map and rose diagram of FIA set 4 trends for the samples taken from the same area as (a). Although FIA sets 1 and 4 and FIA sets 0 and 3 have similar trends, they have been separated and distinguished by relative timing established from core to rim relationships in multi-FIA samples. See text for discussion.

7. Interpretation

7.1. Succession of FIA sets—strong evidence for lack of porphyroblast rotation

The preservation of a consistent succession of five FIA sets across the Pomfret dome is strong evidence that the porphyroblasts did not rotate as they formed, or as the fold formed and was modified by younger deformations. Some samples from each FIA set contain spiral-shaped inclusion trails. Those defining FIA set 0 could have formed by rotation of the garnet porphyroblasts within the matrix foliation. However, those in subsequent sets could not because, as each set developed, it would have caused previously formed FIAs to rotate by the amounts suggested by the curvature of the inclusion trails. The progressive effects of this are shown in Fig. 14. FIA set 0 is rotated about FIA set 1 by up to 180°, the maximum curvature shown by these trails in sections cut at a high angle to the FIA (Fig. 14a). This distribution of FIA set 0 would then have been rotated by up to 270°, the maximum curvature shown by the inclusion trails defining FIA set 2 in sections cut at a high angle to the FIA (Fig. 14b). If FIA set 0 is then rotated about FIA set 3 (Fig. 14c), this would produce an enormous spread of FIA trends for FIA set 0. Rotation of FIA set 1 around FIA sets 2 and 3 is shown in Fig. 14d and e. An enormous spread of these FIAs around the compass would result from the subsequent development of the porphyroblasts with inclusion trails defining FIA set 4. This is not the case. The five FIA sets are tightly constrained and core median rim relationships give consistent relative timing for the development of each set. Therefore, the spiral shaped trails must have formed by overprinting of successive near orthogonal foliations rather than porphyroblast rotation within a shear zone or due to folding (e.g. Bell and Johnson, 1989).

7.2. Fold timing from matrix foliation asymmetry

Across the dome hinge, the change in differentiation asymmetry of S_4 into S_5 (Fig. 7) matches that for an axial plane crenulation cleavage that accompanied dome development (Fig. 15; Williams and Schoneveld, 1981). However, the switch in asymmetry of S_4 on S_3 from limb to limb (Fig. 7) indicates that the dome predated D_4 (Fig. 15a and b) and, therefore, intensified but did not first develop during D_5. In zones of low D_5 strain, S_4 has a sub-horizontal orientation and S_3 is commonly preserved with a sub-vertical orientation (Figs. 4, 6 and 9). The overall coaxial asymmetry associated with the development of S_4 relative to S_3 across the fold (Fig. 15b) suggests that the dome lay close to the core of the orogen with gravitational collapse centred on the dome axis (e.g. Fig. 15b; Bell and Johnson, 1989). This indicates the dome fold is at least as old as D_3 (Fig. 15a). Since S_2 is rarely preserved within the matrix we use below the inclusion trails within porphyroblasts to access the overprinting asymmetries of this and earlier formed foliations.

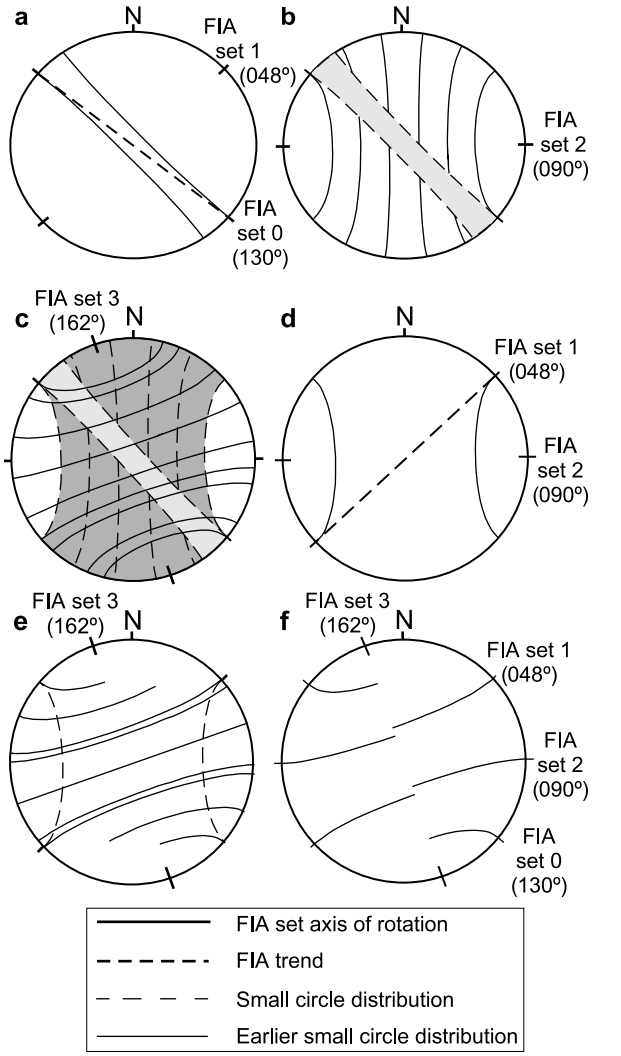

Fig. 14. Stereos showing the effects of rotating successive FIA sets around the mean trend of the next FIA in the succession. (a) Effects of rotating FIA set 0 about FIA set 1 by 180° to produce the maximum curvature recorded by FIA set 1 inclusion trails. (b) Effects of further rotating FIA set 0 around FIA set 2 by 270° to produce the maximum curvature recorded by FIA set 2 inclusion trails. (c) Effects of rotating FIA set 0 around FIA set 3 by 180° to produce the maximum curvature recorded by FIA set 3 inclusion trails. The spread of FIA set 0 data across the stereo net is complete without including the effects of rotation during the development of FIA set 4. ((d) and (e)) Effects of similar rotations on FIA set 1 due to the development of FIA sets 2 and 3. (f) Effects of just rotating previously unrotated FIA sets 0–2 about FIA set 3.

7.3. Fold timing from foliation asymmetry preserved in porphyroblasts

Inclusion trails trapped within porphyroblasts preserve the differentiation asymmetries for the succession of foliations that they represent (Bell et al., 2003). The inclusion trail asymmetry preserved in each sample, and

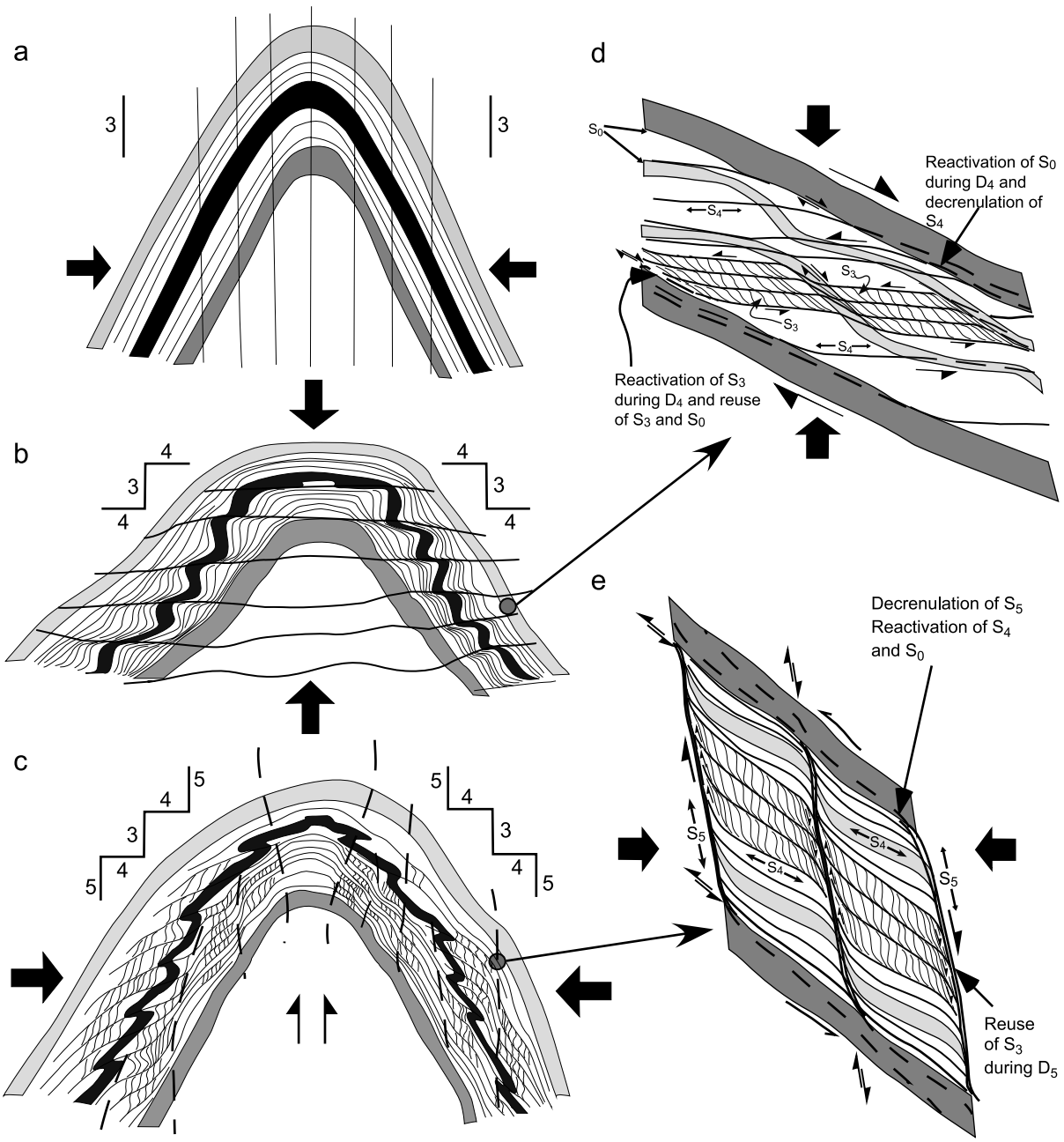

Fig. 15. (a) S_3 unaffected by D_4 and D_5 maintains a sub-vertical geometry, implying upright coaxial folding during D_3 by horizontally directed compression. (b) The overprinting effects of D_4 on S_3 switch asymmetry across the dome indicating predominantly coaxial deformation. (c) S_5 is weakly and heterogeneously but coaxially developed at the dome scale. (d) Reactivation of S_0 during D_4 decrenulates S_3, and rotates S_3 and S_4 into parallelism with S_0. The mirror image of this geometry occurs on the left side of the fold. (e) During D_5, S_4 is rotated further towards S_0, and subsequently reactivation of S_4 results in the decrenulation of S_5, which rotates S_5 parallel to S_0. Shear on S_5 differentiated cleavage will decrenulate S_4 and reuses S_3 as an axial plane foliation. The mirror image of this geometry occurs on the left side of the fold.

separated according to FIA set and limb on the Pomfret dome, shows both asymmetries are present on both limbs in roughly equal amounts (Fig. 11a). An upright fold should show predominantly ACW asymmetries for flat to steep foliation successions on the west limb and CW ones on the east limb as shown in the fold inset in Fig. 11b (Bell and Johnson, 1989). The histograms in Fig. 11b show these asymmetries plotted according to FIA set and whether the sample lies on the east or west limb. FIA set 0 has more CW asymmetries on the west limb and more ACW asymmetries on the east limb, the opposite to that expected for porphyroblasts, which grew syn folding. This may indicate that the fold was present before FIA set 0 began to develop. Bell et al. (2003) showed that porphyroblasts preferentially grow on the limbs of early-formed regional folds where the limb dip vs. the shear sense operating on a newly developing foliation is such that the bedding cannot be reactivated. This relationship is shown on the left limb of the antiform in

Fig. 16a. Porphyroblasts preferentially grow on this limb because all layers are affected by the developing crenulations (Fig. 16a–c) providing sites for porphyroblast growth wherever the bulk composition is suitable at those P–T conditions. However, the right limb can reactivate from the commencement of deformation (Fig. 16d), and some layers with suitable bulk compositions never crenulate, providing fewer sites for porphyroblast growth (Fig. 16d and e; Bell et al., 2003). For both limbs of the Pomfret dome to be dominated by the opposite asymmetries to that shown in the fold inset in Fig. 11b, the shear sense operating on developing vertical foliations would have to switch across the dome hinge in the opposite manner to that which occurred when the fold formed.

FIA set 1 shows a dominance of ACW asymmetries on both limbs. FIA set 2 (Fig. 11b) trends perpendicular to the axial plane, and has no genetic relevance to fold development unless the dome originally formed as an E–W-trending fold that was subsequently shortened into a N–S-trending shape. To test this we plotted the asymmetries from the north to the south half of the dome across an E–W axial plane but the relationship obtained is the inverse to that expected (Fig. 11c). FIA sets 3 and 4 have more ACW asymmetries on the west limb and more CW asymmetries on the east limb (Fig. 11b). The fold could have first formed during the development of either of these FIA sets rather than prior to FIA set 0. We suggest this was not the case for four reasons. (1) The distribution of asymmetries for FIA set 0 suggest that a fold was present prior to the development of the earliest FIA set (e.g. Bell et al., 2003). (2) FIA sets 3 and 4 show the same asymmetry relationships from limb to limb. If the fold formed during the development of FIA set 3, why was the pattern repeated during the development of FIA set 4, or vice versa. (3) The S_4/S_5 matrix differentiation asymmetry matches the fold, yet the fold predates D_5 because S_4 horizontally transects it. Similar structural relationships could have occurred throughout the development of FIA sets 3 and 4. (4) The Chester dome (Fig. 3) along the same hinge line predates all porphyroblast growth (unpublished data).

7.4. Model of development for the Pomfret dome

We interpret that the fold that became the Pomfret dome formed prior to the commencement of porphyroblast growth and was modified by a long succession of events that generally were overall approximately coaxial. It appears to be relatively young because the pervasive matrix schistosity, which postdates most porphyroblasts, is folded together with S_0. However, reactivation of pre-existing foliations, particularly bedding, generally unfolds parasitic folds, decrenulates developing crenulations and rotates previously developed cleavage into parallelism with S_0 (Fig. 2d; Bell, 1986). Reactivation involves shear on S_0 that is antithetic to shear on the newly developing foliation (Fig. 2a) and occurs during deformation partitioning where anastomosing synthetic axial plane shear (Fig. 2b) switches to shear along the bedding (Fig. 2c). Competency differences between beds partitions deformation along S_0 in some layers more than others causing decrenulation of newly developing foliations and the rotation of crenulated foliation into parallelism with

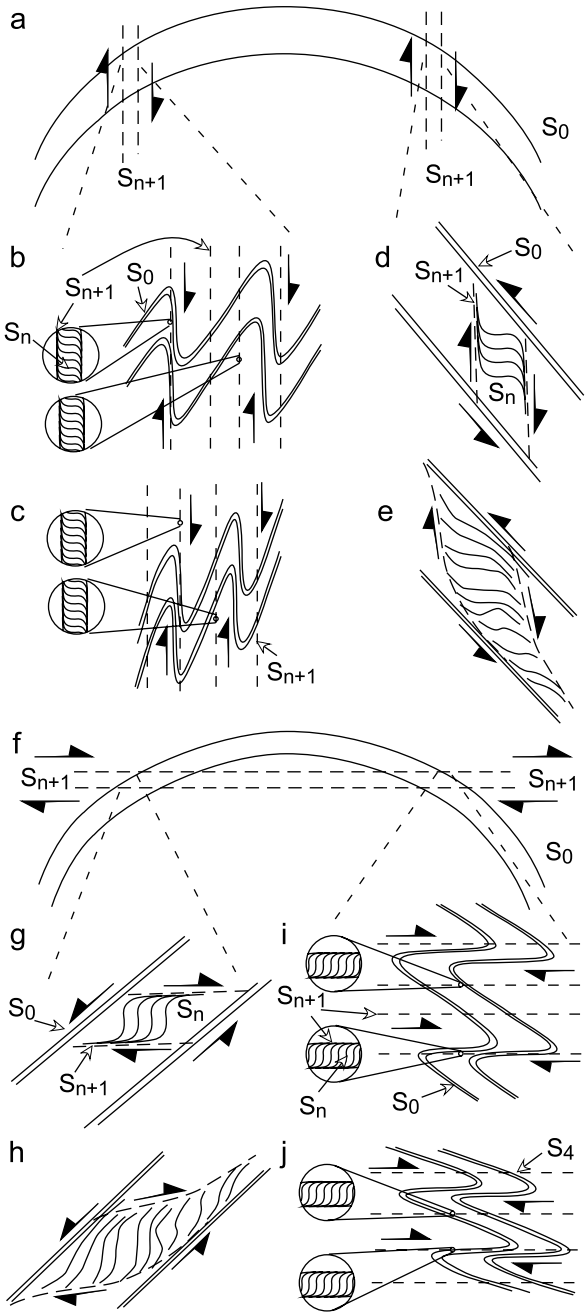

Fig. 16. Where the asymmetry of curvature of S_n into S_{n+1} does not change across an upright fold (a), one limb ((b) and (c)) cannot reactivate and S_{n+1} intensifies until deformation ceases. On the other, S_0 reactivates from the commencement of D_{n+1} in some layers preventing crenulation and reducing sites for porphyroblast growth ((d) and (e); see Bell et al., 2003). Where horizontal S_{n+1} cuts a vertical fold (f) and the CW asymmetry of S_n into S_{n+1} does not change from limb to limb, reactivation of S_0 occurs locally on the left limb (g) from the start of D_{n+1}. This causes unfolding of crenulated S_n and rotates or destroys newly developing S_{n+1} (h). On the right limb, S_0 cannot reactivate and S_{n+1} develops (i) and then intensifies (j) as the deformation proceeds.

S_0 (Fig. 2d; Bell, 1986). Where an upright fold is overprinted by a sub-horizontal foliation, S_0 can reactivate on one (Fig. 16f–h) or both (Fig. 15b and d) limbs from the commencement of deformation. In Fig. 16f–j the curvature of S_n into S_{n+1} does not change asymmetry across the fold and reactivation of S_0 is possible on the left (Fig. 16g and h) but not the right (Fig. 16i and j) limb. In Fig. 15b and d the curvature of S_3 into S_4 switches asymmetry across the fold in a manner that allows reactivation to occur on both limbs. During D_4 this resulted in decrenulation of S_3, the local destruction of developing S_4, and/or the rotation of relics of S_4 into sub-parallelism with S_0 around the domal fold (Fig. 15d). D_5 further rotated any oblique remains of S_4 towards S_0 because S_5 formed axial planar to the dome fold and switches differentiation asymmetry across it (Fig. 15c and e). Reactivation during D_5 further decrenulated any remains of D_4 crenulations and locally S_3 was reused as an axial plane foliation as shown in Fig. 15e (e.g. Davis and Forde, 1994; Davis, 1995). D_5 would have added to the amplitude of the dome fold (Fig. 15c) after the decrease in amplitude that resulted from the effects of gravitational collapse that accompanied D_4 and the development of sub-horizontal S_4 (Fig. 15b; e.g. Bell and Johnson, 1989, 1992).

This succession of events from D_3 to D_5 may reflect much of the progressive history of development of foliations in the dome from when it first formed, but particularly during the porphyroblast growth accompanying the development of FIA sets 3 and 4. At various stages in the deformation history the differentiation asymmetry associated with the development of a horizontal foliation would not have changed across the fold hinge, as described above, and one limb of the fold could have reactivated (Fig. 16g and h) while the other continued to develop a new cleavage (Fig. 16i and j; e.g. Bell et al., 2003). Infrequent preservation of S_2 suggests that reactivation occurred extensively during D_2, similar to that in D_4. Such overprinting would modify the geometry of the dome fold without developing major refolds (see also Adshead-Bell and Bell, 1999; Bell et al., 2003).

8. Discussion

8.1. Lack of porphyroblast rotation

An external reference frame is needed to quantitatively test all aspects of both rotation and non-rotation models for porphyroblast behaviour during ductile deformation because the latter model invokes the role of gravitational collapse in foliation development (Bell and Johnson, 1989; Aerden, 1994, 2004). Consequently, all FIAs were measured using thin sections oriented relative to the vertical as well as with respect to geographic co-ordinates. The consistency of the trends of the five successive FIA sets across the area, as well as on both limbs of the Pomfret dome (compare Figs. 12–14), indicates that the porphyroblasts did not rotate as they formed, or during the modification of the dome that accompanied subsequent ductile deformations. The simple consistent succession of FIAs observed would be impossible if the porphyroblasts had rotated (e.g. Fig. 14).

8.2. Fold mechanisms

The precursor structure that eventually became the Pomfret dome may have initiated prior to the growth of porphyroblasts that preserve FIA set 0. Determining what mechanism operated at that stage of dome development is not possible. However, a very extensive history of deformation, accompanied by multiple phases of foliation formation and porphyroblast growth, postdated this stage of the dome's development. The precursor fold would have been modified in shape by each of these events in a similar manner to that revealed by the rotation of matrix S_4 from limb to limb. Yet successive sets of FIAs do not change trend from limb to limb. This suggests a solution to the mechanism of folding during each of these events. Traditionally, folding mechanisms have been kinematically divided into four end member models, which, if operating independently, will rotate porphyroblasts (Fig. 17; Williams and Jiang, 1999; Jiang, 2001). They are pure shear, which rotates elliptical porphyroblasts lying oblique to the shortening direction, tangential longitudinal strain, flexural slip or flexural flow and shear folding (e.g. Ramsay, 1967, pp. 392–397; Hobbs et al., 1976, pp. 183–195). These mechanisms vary in how they accommodate strain, resulting in differing fold geometries, microstructures and porphyroblast behaviour (Williams and Jiang, 1999). Jiang (2001) argued that all possible deformation paths leading to fold development could be represented by some combination of these selected end members operating both temporally and spatially and varying from domain to domain during fold development. However, he did not consider the progressive bulk inhomogeneous shortening folding mechanism of Bell and Hickey (1997). Each of the end member fold mechanisms involving pure shear (for non spherical porphyroblasts), tangential longitudinal strain, and flexural slip or flexural flow rotate porphyroblasts in such a way that core FIAs must show a large range of orientations around the Pomfret dome, and, therefore, do not explain the porphyroblast behaviour that we have observed.

8.2.1. Combinations of end member fold mechanisms—buckling

Porphyroblast rotation has been modelled by sequential superposition of the end-member fold models (Williams and Jiang, 1999) combined with the mechanical effects of differing competency between folded layers (Jiang, 2001). Since tangential longitudinal strain is considered to have a negligible effect in multilayer folding, a typical combination of end members used involves early coaxial shortening involving pure shear, layer parallel shear by flexural slip or

flexural flow, with coaxial flattening of the fold (pure shear) once a critical limb dip is reached. Relative rotation occurs with respect to S_0 (the layer undergoing layer parallel shear) and S_1 (the developing axial plane foliation). Williams and Jiang's (1999) modelling of rotation by these end member models suggested that after initial pure shear shortening, the effect of layer competency on porphyroblast rotation increased during flexural slip or flexural flow folding, but decreased with later pure shear flattening. Jiang (2001) concluded that rotation with respect to the axial plane is small, $\ll 45°$, and that, therefore, observations that porphyroblasts appear to have rotated little across a fold hinge are compatible with his theoretical predictions. They concluded that inclusion trails in porphyroblasts preserving greater than 90° of curvature must have formed by rotation of the porphyroblasts within a shear zone. However, no discrete shear zones or successions of shear zones are preserved at the sample locations around the Pomfret dome (Fig. 5a) that can be used to explain the succession of five FIA trends that we have identified. Furthermore, the theoretical modelling of Williams and Jiang (1999) and Jiang (2001):

1. Only looks at partitioning between layers of different initial competency,
2. Takes no account of partitioning of vorticity between layers and cleavage domains with the growth of porphyroblasts,
3. Is solely based on inclusion trail curvature relative to limb dip for the formation of a single fold,
4. Only considers relative rotation of porphyroblasts with respect to an external foliation.

FIA sets 0–3 are commonly truncated by the matrix foliation and hence predate it. Consequently, porphyroblast rotation must be considered between the different FIA sets with respect to a reference frame that includes geographical coordinates and the vertical. If their modelling was correct, the succession of five FIA sets recorded in this study represent five different axes of rotation. In any one FIA set, the variation of inclusion trail curvature ranges up to 270°. This curvature represents the finite rotation of porphyroblasts within a layer, and therefore the vorticity history within layers (Jiang, 2001). Some inclusion trails defining core FIAs are surrounded by up to 180° of inclusion trail curvature defining differently trending median and rim FIAs. Staircase-shaped inclusion trail geometries defining single FIAs are also common. This data cannot be readily explained by a combination of end member fold models.

8.2.2. Axial plane shear fold models

Fold models involving a component of axial plane shear

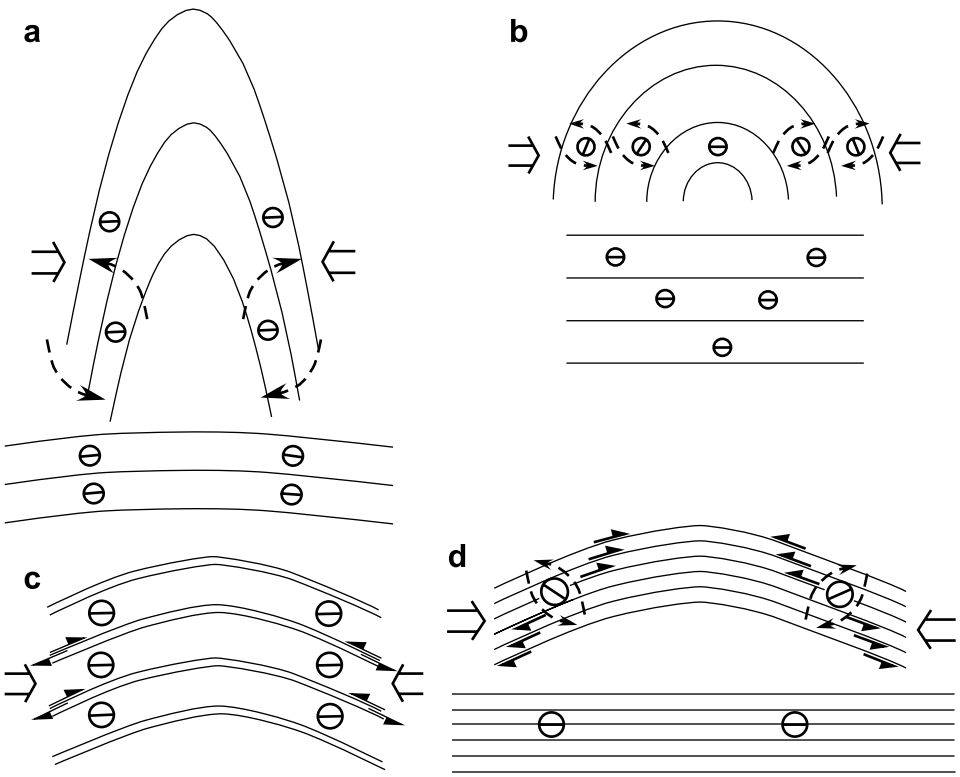

Fig. 17. Schematic diagrams illustrating the key elements of fold mechanisms that would increase the variation of FIA trends as described within the text. (a) Pure shear involves homogeneous coaxial shortening with no rotation relative to geographical co-ordinates. (b) Tangential longitudinal strain where finite strain decreases outward from the fold hinge, and therefore porphyroblast rotation decreases from the inner to the outer arc. (c) Flexural slip and (d) flexural flow where the folded layers experience simple shear parallel to the folded layer resulting in vorticity induced rotation of porphyroblasts that is opposite to spin on the fold limbs.

can preserve the same FIA orientations on both limbs of the Pomfret dome (Fig. 18) because the progressive shearing component of the deformation is partitioned into the cleavage seams and the porphyroblasts lie within the microlithons. In such models, provided the porphyroblasts do not internally deform, they may not rotate. Three types of fold models have been proposed that involve axial plane shear. They include the card deck model (shear folding), where there is no component of bulk shortening, shear combined with homogeneous shortening of the microlithons (clay brick model) and progressive bulk inhomogeneous shortening (PBIS) where progressive shearing and shortening are partitioned heterogeneously through the deforming mass.

The *card deck model* (Fig. 18a) could preserve preexisting FIA trends if the porphyroblasts lay in undeformed microlithons between zones of shearing (i.e. entirely within the cards; Fig. 18a). The slip is partitioned beyond the microlithons and the porphyroblasts do not rotate. However, this model is precluded because no component of shortening is possible, yet bulk shortening accompanies orogenesis in many tectonic environments.

De Sitter's (1956) *clay brick model* could preserve preexisting FIA trends if the porphyroblasts lie in the microlithons (the clay bricks) between cleavage seams, along which shear occurs parallel to the axial plane. This model differs from the card deck model in that the microlithons are coaxially shortened during folding (Fig. 18b). However, ellipsoidal porphyroblasts (e.g. staurolite, kyanite and some garnets) lying oblique to the microlithon boundaries would rotate in this model and, therefore, it is precluded (e.g. Bell and Hickey, 1997; Hickey and Bell, 2001).

Bell's (1981) model of *progressive bulk inhomogeneous shortening (PBIS)* has porphyroblasts growing within and subsequently controlling the development of zones of progressive shortening. These zones are the microlithons between differentiated crenulation cleavage seams, but are also present in rocks where all such microlithons have been destroyed by reactivation (Bell, 1986). If there is no internal deformation of the porphyroblasts, then they do not rotate because the shearing component of the deformation is partitioned entirely into zones that can deform and which anastomose around the porphyroblasts (Bell and Hickey, 1997). Consequently, zones of progressive non-coaxial shearing strain and volume loss surround zones of essentially coaxial progressive shortening or no strain (Fig. 18c; Bell, 1981). This model requires successive deformation by horizontal compression and vertical collapse to generate the inclusion trail geometries found within the rocks described herein (Bell and Johnson, 1989; Aerden, 1994, 1995). Such a model requires a more complicated deformation history for the development of many regional scale folds. Where old folds are preserved, they will have been opened or tightened by many successive events (Adshead-Bell and Bell, 1999; Hickey and Bell, 2001; Bell et al., 2003).

8.3. Reactivation and reuse of foliations during folding

During folding by progressive bulk inhomogeneous shortening, rigid porphyroblasts are displaced but not

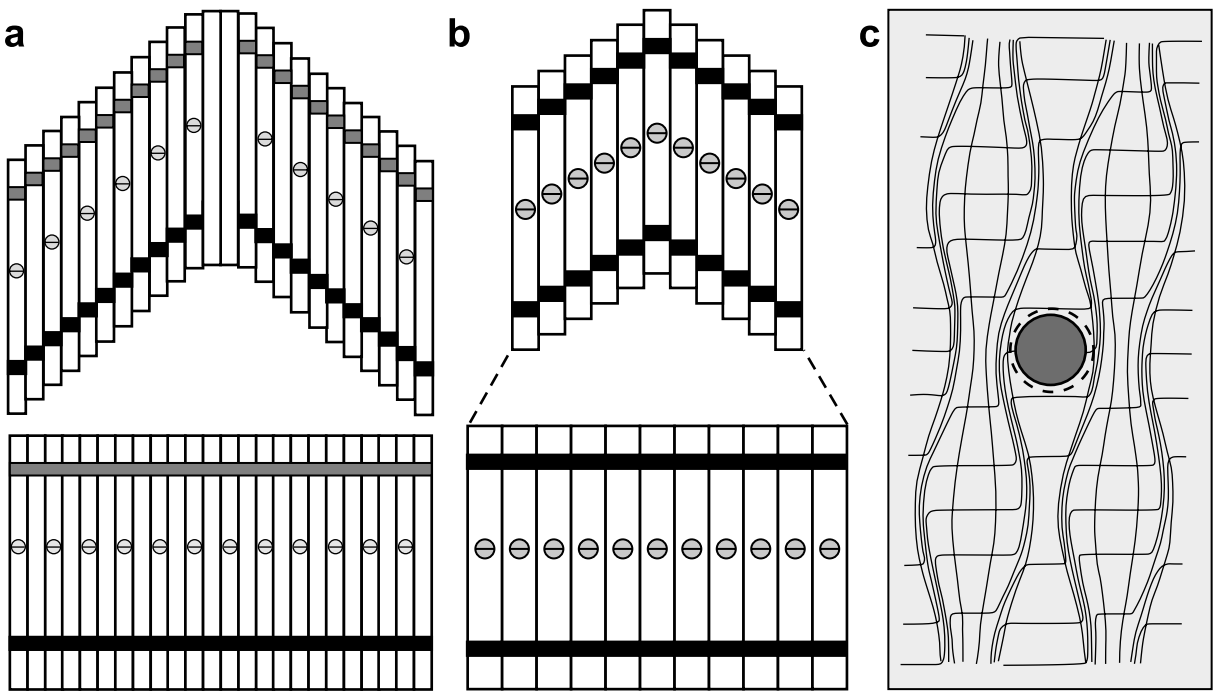

Fig. 18. Schematic diagrams illustrating the key elements of fold mechanisms that would maintain FIA orientations as discussed within the text. (a) Slip folding (card deck model). (b) Clay brick model of De Sitter (1956). (c) Progressive bulk inhomogeneous shortening (PBIS).

rotated as progressive shearing occurs sub-parallel to the axial plane (Fig. 2a and b) or along reactivated bedding (Fig. 2a and c). Because of the early development of the fold that became the Pomfret dome, reactivation of one or both of the limbs of this fold was possible from the commencement of all subsequent deformation events, independent of whether these events involved horizontal shortening (Figs. 15a,c,e and 16a–e) or vertically directed gravitational collapse and spreading (Figs. 15b,d and 16f–j). For example, D_5 did not develop a strong foliation, and only locally formed a differentiated crenulation cleavage, S_5, suggesting this event was weakly developed relative to D_4. However, this deformation was accompanied by reactivation of S_0 on the limbs of the dome and decrenulation (Fig. 15c and e), rather than continued S_5 development (Bell, 1986) making D_5 appear a weaker event than it actually was. D_4 also involved strong reactivation of the folded foliation, and because S_4 lay closer to the overall form surface of the dome, D_4 appears to be a stronger event than D_5 without this necessarily being the case. The pre-matrix history found within porphyroblasts is similar to that found in the matrix. No single deformation event after the dome first formed was strong enough to disrupt its geometry as currently exposed. Consequently, throughout the domes history, as each new crenulation cleavage began to develop in response to the most recent orthogonal switch in the direction of bulk shortening, any foliation lying oblique to bedding that had formed in the previous deformation, or which still remained relatively unscathed from even earlier deformations, was decrenulated on at least one limb of the dome because of reactivation of the bedding (Figs. 15d,e and 16e,g,h; see fig. 13a–c in Bell et al., 2003). Decrenulation destroys newly developing crenulation cleavages plus rotates any non-destroyed relics of it towards the bedding as shown in Figs. 2d and 15d,e and 16d,e,g,h. Decrenulation also rotates any remains of earlier formed foliations towards parallelism with bedding as shown in Fig. 16c and d. Thus foliations oblique to bedding tend to only survive the effects of two or three younger deformations if they were not trapped within porphyroblasts. The youngest matrix foliations survive because the ductility of the rock mass rapidly decreases as it is lifted up through the orogenic pile.

8.4. Formation of spiral inclusion trails during folding rather than during shearing

Williams and Jiang (1999) argued that spiral-shaped inclusion trails could only develop within a shear zone as curvature of inclusion trails greater than 90° could not form during folding. They ignored the cumulative effect of successive deformations (Stallard and Hickey, 2001; Bell and Chen, 2002). Superb spiral-shaped inclusion trails have formed throughout the Pomfret dome region during multiple successions of events that on the bulk scale of the dome were both coaxial and non-coaxial. Both asymmetries are common (Fig. 11). This history creates an overwhelming problem for the Williams and Jiang (1999) concept of spiral inclusion trail development because this dome predated most if not all of the porphyroblast growth, yet has been preserved while successive generations of spiral shaped trails formed. There are five different generations of spiral shaped inclusion trails in these rocks that get progressively younger in age. According to the Williams and Jiang concept, sufficient porphyroblast rotation to explain the 120–270° of apparent curvature of inclusion trails defining any one of the FIA sets present in these rocks, requires the development of a long lived shear zone that post-dated dome development. In fact their model requires a succession of at least five shear zones, each producing 120–270° of apparent curvature of inclusion trails to explain the succession and progressively younger ages of the FIA trends (Bell and Welch, 2002). Each shear zone would have cut through and displaced portions of the dome. These shear zones should have been folded, cut and displaced by successive younger shear zones formed during the development of subsequently generated FIA sets. There is no evidence for such a history preserved in these rocks. The dome is a relatively simple structure and these dome truncating shear zones are not present. Although this cannot be explained by Williams and Jiang's (1999) model for spiral inclusion trail development, it can be readily explained by Bell and Johnson's (1989) model.

Acknowledgements

We acknowledge funding provided by the School of Earth Sciences at James Cook University and the Australian Research Council that enabled the research to be done. We also acknowledge the JCU research facilities. The Departamento de Geodinamica at the Universidad de Granada provided facilities that allowed a major revision of this manuscript to be made.

References

Adshead-Bell, N.S., Bell, T.H., 1999. The progressive development of a macroscopic upright fold pair during five near-orthogonal foliation-producing events: complex microstructures vs. a simple macrostructure. Tectonophysics 306, 121–147.

Aerden, D.G.A.M., 1994. Kinematics of orogenic collapse in the Variscan Pyrenees deduced from microstructures in porphyroblastic rocks from the Lys–Caillaouas Massif. Tectonophysics 238, 139–160.

Aerden, D.G.A.M., 1995. Porphyroblast non-rotation during crustal extension in the Variscan Lys–Caillaouas Massif, Pyrenees. Journal of Structural Geology 17, 709–725.

Aerden, D.G.A.M., 2004. Correlating deformation in Variscan NW-Iberia using porphyroblasts; implications for the Ibero–Armorican Arc. Journal of Structural Geology 26, 177–196.

Armstrong, T.R., Tracy, R.J., Hames, W.E., 1992. Contrasting styles of Taconian, Eastern Acadian and Western Acadian metamorphism, central and western New England. Journal of Metamorphic Geology 10, 415–426.

Armstrong, T.R., Walsh, G.J., Spear, F.S., 1997. A transect across the Connecticut Valley sequence in east-central Vermont: geochronology and Nd, O, Pb, and Sr isotopic constraints on the origin of Acadian granitic rocks. In: Grover, T.W., Mango, H.N., Haschohr, E.J. (Eds.), Guidebook to Field Trips in Vermont and Adjacent New Hampshire and New York. New England Intercollegiate Geological Conference, Annual Meeting, 89th, Rutland, Vermont, A6-1-56.

Bell, T.H., 1981. Foliation development: the contribution, geometry and significance of progressive bulk inhomogeneous shortening. Tectonophysics 75, 273–296.

Bell, T.H., 1986. Foliation development and refraction in metamorphic rocks: reaction of earlier foliations and decrenulation due to shifting patterns of deformation partitioning. Journal of Metamorphic Geology 4, 421–444.

Bell, T.H., Chen, A., 2002. The development of spiral-shaped inclusion trails during multiple metamorphism and folding rather than in shear zones. Journal of Metamorphic Geology 20, 397–412.

Bell, T.H., Hayward, N., 1991. Episodic metamorphic reactions during orogenesis: the control of deformation partitioning on reaction sites and duration. Journal of Metamorphic Geology 9, 619–640.

Bell, T.H., Hickey, K.A., 1997. Distribution of pre-folding linear movement indicators around the Spring Hill Synform, Vermont: significance for mechanism of folding in this portion of the Appalachians. Tectonophysics 274, 275–294.

Bell, T.H., Johnson, S.E., 1989. Porphyroblast inclusion trails: the key to orogenesis. Journal of Metamorphic Geology 7, 279–310.

Bell, T.H., Johnson, S.E., 1992. Shear sense: a new approach that resolves conflicts between criteria in metamorphic rocks. Journal of Metamorphic Geology 10, 99–124.

Bell, T.H., Rubenach, M.J., 1983. Sequential porphyroblast growth and crenulation cleavage development during progressive deformation. Tectonophysics 92, 171–194.

Bell, T.H., Welch, P.W., 2002. Prolonged Acadian orogenesis: revelations from foliation intersection axis (FIA) controlled monazite dating of foliations in porphyroblasts and matrix. American Journal of Science 302, 549–581.

Bell, T.H., Forde, A., Wang, J., 1995. A new indicator of movement direction during orogenesis. measurement technique and application to the Alps. Terra Nova 7, 500–508.

Bell, T.H., Hickey, K.A., Upton, G.J.G., 1998. Distinguishing and correlating multiple phases of metamorphism across a multiply deformed region using the axes of spiral, staircase and sigmoidally curved inclusion trails within garnet. Journal of Metamorphic Geology 16, 767–794.

Bell, T.H., Ham, A.P., Hickey, K.A., 2003. Early formed regional antiforms and synforms that fold younger matrix schistosities: their effect on sites of mineral growth. Tectonophysics 367, 253–278.

Bradley, D.C., 1983. Tectonics of the Acadian Orogeny in New England and adjacent Canada. Journal of Geology 91, 381–400.

Davis, B.K., 1995. Regional-scale foliation reactivation and re-use during formation of a macroscopic fold in the Robertson River Metamorphics, north Queensland, Australia. Tectonophysics 242, 293–311.

Davis, B.K., Forde, A., 1994. Regional slaty cleavage formation and fold axis rotation by reuse and reactivation of pre-existing foliations: the Fiery Creek Slate Belt, north Queensland. Tectonophysics 230, 161–179.

De Sitter, L.U., 1956. Structural Geology, McGraw-Hill, New York, 552pp.

Doll, C.G., Cady, W.M., Thompson, J.B., Jr., Billings, M.P., 1961. Centennial geologic map of Vermont. Vermont Geological Survey, scale 1:250000.

Gray, D.R., 1979. Microstructure of crenulation cleavages: an indication of cleavage origin. American Journal of Science 279, 97–128.

Hayward, N., 1990. Determination of early fold axis orientations within multiply deformed rocks using porphyroblasts. Tectonophysics 179, 353–369.

Hickey, K.A., Bell, T.H., 2001. Resolving complexities associated with the timing of macroscopic folds in multiply deformed terrains The Spring Hill synform, Vermont. Bulletin of the Geological Society of America 113, 1282–1298.

Hobbs, B.E., Means, W.D., Williams, P.F., 1976. An Outline of Structural Geology, Wiley and Sons, New York, 571pp.

Hueber, F.M., Bothner, W.A., Hatch, N.L. Jr, Finney, S.C., Aleinikoff, J.N., 1990. Devonian plants from southern Quebec and northern New Hampshire and the age of the Connecticut Valley Trough. American Journal of Science 290, 360–395.

Jiang, D., 2001. Reading history of folding from porphyroblasts. Journal of Structural Geology 23, 1327–1335.

Lyons, J.B., 1955. Geology of the Hanover Quadrangle, New Hampshire, Vermont. Bulletin of the Geological Society of America 66, 106–146.

Osberg, P.H., Tull, J.G., Robinson, P., Hon, R., Butler, J.R., 1989. The Acadian Orogen. In: Hatcher, R.D. Jr, Tomas, W.A., Viele, G.W. (Eds.), The Appalchian–Ouachita Orogen in the United States, The Geology of North America, F-2., pp. 179–232.

Ramsay, J.G., 1967. Folding and Fracturing of Rocks, McGraw-Hill, New York, 568pp.

Stallard, A.R., Hickey, K.A., 2001. Shear zone vs. folding origin for spiral inclusions in the Canton Schist. Journal of Structural Geology 23, 1845–1864.

Twiss, R.J., Moores, E.M., 1992. Structural Geology, W.H. Freeman and Co, UK, 532pp.

White, W.S., Jahns, R.H., 1950. Structure of central and east-central Vermont. Journal of Geology 58, 170–220.

Williams, P.F., Jiang, D., 1999. Rotating garnets. Journal of Metamorphic Geology 17, 367–378.

Williams, P.F., Schoneveld, C., 1981. Garnet rotation and the development of axial plane crenulation cleavage. Tectonophysics 78, 307–334.